UNIVERSIDAD DE CONCEPCIÓN
FACULTAD DE CIENCIAS FÍSICAS Y MATEMÁTICAS

OCTUPOLE DEFORMATION IN SOME RADIUM ISOTOPES USING THE *spdf*-IBM-1

Por: Pedro Alexander Contreras Corral

Tesis presentada a la Facultad de Ciencias Físicas y Matemáticas de la Universidad de Concepción para optar al grado académico de Magíster en Ciencias con Mención en Física

Marzo 2024
Concepción, Chile

Profesor Guía: Dr. José Barea Muñoz

A quienes fueron parte de este proceso, especialmente desde el inicio.

AGRADECIMIENTOS

Muchas personas han sido parte fundamental de este proceso, y sería imposible nombrarlas a todas. Sin embargo, haré el intento de mencionar a algunas de las más relevantes.

En primer lugar, agradecer a mi mamá y mi papá, quienes desde pequeño me inculcaron el gusto por aprender, aún sin tener siempre los medios para responder mis preguntas. Por su dedicación en mi educación formal, el apoyo en los momentos difíciles que viví en ella, y la preocupación de que yo pudiera asistir a la Universidad, independiente de la situación en que estuviéramos viviendo. Más aún, por su apoyo al momento de decidir estudiar esta carrera, y que pese al desconocimiento que tenían de ella, hicieron todo lo que estuviera en sus medios para que pudiese estudiar con tranquilidad.

Académicamente, debo agradecer sobre todo a mi guía de tesis, el Dr. José Barea, por haber confiado en mí desde cuando me encontraba buscando un tópico de investigación y durante todo el proceso, incluyendo la creación de presentaciones para asistir a eventos científicos como el XXIII Simposio Chileno de Física o la CGS17 en Francia. Quisiera también agradecer a Omar Vallejos, mi compañero de tutor, por su constante apoyo en el trabajo de tesis y sus aportes desde su experiencia en programación y en la estructura nuclear.

No debo dejar de mencionar tampoco a las y los docentes del Departamento de Física, cuyas experiencias fueron parte de mi formación académica. En especial, al Dr. Julio Oliva por ser siempre una fuente de ayuda para mis consultas y por la confianza que en el tiempo depositó en mi. Al Dr. Hernán Astudillo, con quien trabajé de manera cercana durante los tres años que estuve en el Centro de Estudiantes, por su disposición a escucharnos y su preocupación por el funcionamiento de la carrera. A la Dra. Noelia Benito por permitirme introducirme, aunque fuera brevemente, en experiencias experimentales, descubriendo que no soy tan nulo en estas como originalmente creía. En fin, agradecer en general a todas y todos los docentes del Departamento con quienes compartí clases, actividades o simplemente conversaciones, pues todas estas experiencias fueron parte de mi formación académica.

Debo también agradecer a mis compañeros de carrera, quienes confiaron en mí para representarlos durante tres años, entre quienes existen personas cuya amistad merece especial mención. En primer lugar, agradecer a José Huenchual, compañero de trabajos

durante toda mi vida académica, en quien sé que puedo confiar como compañero, como persona y como amigo. Agradezco a Gerardo Millar y a Tomás Troncoso por ser parte del equipo que formamos junto con José, tanto para hacer tareas, para apoyo moral, y para las noches de Civ VI, Minecraft, Patojuego, entre otras. A Bárbara Candia, por ser una mentora en lo que respecta a cómo enfrentarme a las instancias de representación, y por ser una buena amiga. A Ignacio Ormazábal, Jorge Escandón, Nicolás Parra y Lorena Sepúlveda por la buena compañía durante el Magíster, por las conversaciones que surgieron, los almuerzos y por supuesto, los cafés proporcionados por Nico.

Agradecer a nuestras secretarias, Julia Herrera, Soledad Daroch, Nilsa García y Patricia Luarte, pues más de una vez debí molestarlas con montones de consultas o solicitudes, y siempre tuvieron la mejor disposición para tratarlas.

A las amistades con las que pude compartir durante mis estudios. Entre otros, Adheris C., Alejandro S., Luis U., Jossef G., Catalina P., Montserrat A., Camilo A., Martín S., Martín Q., Arelly N., Macarena S., Jorge G., Consuelo B., Lixin L., Fernanda M., Lissette L., Amaro D., Sebastián R., Javiera A., Danilo R., Nicol G., Silvana F., Sofía G., Scarlett R., Aníbal N., Marcel Y., Pablo R.

Debo también agradecer a quienes fueron parte de mi formación inicial, sin la cual no podría estar en este punto, mis profesoras y profesores durante mi etapa escolar. Profesoras Silvana, Carolina, Mariana, Rossana, Andrea, Valeria, Ana Luisa, Kiomara, Sandra, Claudia G., Paulina, Carla, Rosita, Claudia H., y especialmente a mis profesoras de física, Luisa y Camila, quienes sin saberlo lograron enamorarme de esta área. También a mis profesores, Bernardo, Cannobbio, Gonzalo, Hernán, y especialmente a mis profesores de historia, César y Nelson, quienes me ayudaron en la formación de pensamiento crítico y permitirme ser la persona que soy hoy.

Agradecer a quienes de distintas maneras trabajan por hacer del conocimiento algo accesible para todos, y a quienes buscan poner en la opinión pública los problemas estructurales del modelo educativo y contribuir con distintos avances, por pequeños que sean, a solucionar estos problemas, pues nos permiten ir en la dirección correcta.

Por último, agradecer al Ministerio de Educación por el financiamiento de mis estudios de pregrado mediante la Beca Bicentenario y la Gratuidad, a la Agencia Nacional de Investigación y Desarrollo por financiar parcialmente esta tesis mediante el FONDECYT N° 1190489 y la Beca de Magíster Nacional N° 22231691, y a la Universidad de Concepción por haberme otorgado la Beca de Articulación Pregrado-Postgrado.

Resumen

En esta tesis hemos realizado un estudio espectroscópico de carácter fenomenológico de los grados de libertad octupolares presentes en la cadena de isótopos de radio $^{216-228}$Ra en el contexto del Modelo de Bosones *spdf* en Interacción (*spdf*-IBM). Este carácter se debe al desarrollo de una rutina de minimización para la obtención de los parámetros del hamiltoniano utilizado. En particular, analizamos sus espectros de energía, transiciones electromagnéticas entre estados de igual ($B(E2)$) y distinta paridad ($B(E1), B(E3)$), y momentos multipolares, pudiendo comparar estos resultados con recientes mediciones experimentales.

El interés en estos isótopos se basa en la presencia de deformación octupolar en ellos, lo que se relaciona con los momentos dipolares eléctricos atómicos, cuya medición puede poner a prueba la simetría CP del Modelo Estándar de la Física de Partículas.

Keywords – Modelo de bosones en interacción, deformación octupolar, transiciones electromagnéticas

Abstract

In this thesis we have made a spectroscopic study, of phenomenological nature, of the octupole degrees of freedom present in the radium isotopic chain $^{216-228}$Ra in the context of the *spdf* Interacting Boson Model (*spdf*-IBM). The phenomenological nature is due to the developement of a minimization routine for obtaining the parameters of the chosen hamiltonian. In particular, we analyze their energy spectra, electromagnetic transitions between states of the same ($B(E2)$) and different parity ($(E1), B(E3)$), and the multipole moments, comparing these results with recent experimental measurements.

The interest on these isotopes emerges from the presence of octupole deformation in them, which relates with the atomic electric dipole moments, whose measurements may put to test the CP symmetry of the Standard Model of Particle Physics.

Keywords – Interacting boson model, octupole deformation, electromagnetic transitions

Contents

List of Tables

List of Figures

Chapter 1

Introduction

The nuclear many body problem still presents many challenges and difficulties to be completely solved. One of these difficulties is the fact that there is not an analytical expression for the nuclear forces between nucleons in the same manner as there is the Coulomb law in electric systems. These nuclear forces are a remainder from the interaction between the quarks composing the inner structure of those nucleons. Another problem that arises is the fact that heavy nuclei possess nucleons of the order of 200, a number too small to use statistical methods, and too large for our current computational capacity to use first principle methods, so we can not speak about a Nuclear Theory, but we can talk about several Nuclear Models that are suitable on nuclei of different sizes.

One of these models is the Shell Model, which suggest that the inner structure of the nucleus is similar to the electronic structure of atoms, with nucleons filling different shells of the nucleus, with various orbitals in each shell. Similar to the atomic case, in which the noble gases are exceptionally stable compared to their neighbors, there are special values of the number of protons and neutrons (Z and N, respectively) for which a given nucleus will be specially stable, those being the nuclear magic numbers, 2, 8, 20, 28, 50, 82, 126, ..., giving the nucleus a spherical shape.

Continuing with the comparisons with the electronic structure of the atom, the nucleons of an unclosed shell are referred to as valence nucleons, and the interactions between them will origin different correlations that may cause deviations in the nuclear shape away from the spherical. Some specific deformations

that may arise are the quadrupole and octupole deformations, that may be detected based on the measurements of the asociated multipole moments, those being a direct evidence of them, as well as this may be infered based on the study of the energy spectra of these nuclei.

One particular model that allow us to realize this studies is the Interacting Boson Model (IBM), which allows to reproduce the low-lying energy levels of even-even nuclei and to study some of their properties, such as the previously mentioned multipole moments, by studying the electromagnetic transitions between different states. The model, in general terms, takes the valence nucleons of the Shell Model and considers that pairs of them are able to couple with given good values of angular momentum. One particular version of this model, the *spdf*-IBM-1, considers the existence of bosons with negative parity, and they allow the description of phenomena asociated with octupole deformations, like the presence of low-energy states with negative parity, and non-zero dipole and octupole electric transition rates between states of different parity. This octupole deformation has been one of the most studied topics in nuclear structure in recent years [1–3].

The rare-earth (Z $\sim$ 56, N $\sim$ 88) and actinide (Z $\sim$ 88, N $\sim$ 134) regions of the nuclear chart show a bigger presence of octupole phenomena [1], so the experimental and theoretical efforts have been centered in the elements present in those regions, such as Ba, Ce, Sm or Nd in the rare-earth, and Th, U, Pu or Ra in the actinides.

During the last decade, major experimental breakthroughs have been achieved in the measurement of evidence of vibrational deformation in radon isotopes [4] and permanent deformation in radium isotopes [5, 6]. New theoretical work has made use of this results, like Nomura *et al.* in Ref. [7] via the *sdf*-IBM-1 and Vallejos and Barea in Ref. [8] via the *spdf*-IBM-2, but there has not been new works that make use of the *spdf*-IBM-1 since the work of Zamfir an Kusnezov in Ref. [9], which was done before these measurements.

Taking into account the previous discussion, we think that the Interacting Boson Model has been proven to provide an accurate description of the low energy states of heavy nuclei. The current state of computational devices also allow us to eliminate previous restrictions in the number of negative-parity bosons imposed in the calculations of Zamfir and Kusnezov [9], which in combination with the

new experimental data available and the election of an adequate hamiltonian, we hipothesize that our approach will allow us to reproduce the experimentally observed octupole phenomena in the radium isotopic chain, as well to make predictions in those nuclei that do not possess experimental data avaliable.

The general objective of the present work is to study the octupole phenomena present in some elements of the even-even Radium isotopic chain in the framework of the *spdf*-IBM-1, serving as an update of the previous work made by Zamfir and Kusnezov. In particular, we aimed to

1. Make numerical calculations to find a set of hamiltonian parameters for each nuclei in the $^{216-226}$Ra isotopic chain that is able to reproduce fairly well the experimental data available.
2. Identify the presence or absence of octupole deformation in the studied Radium isotopes.
3. Study the effects that the interaction terms in our hamiltonian have on the description of octupole-deformed nuclei.

This Thesis is divided as follows: In chapter 2 we present the theoretical aspects behind the nuclear deformation, specially about the quadrupole and octupole deformation, as well as some aspects about the Interacting Boson Model. In chapter 3 we discuss the methods that we worked with, each one of them answering to one of the objectives previously listed. In chapter 4 we show and discuss the results of the study of octupole phenomena in the case of the even-even Radium isotopic chain. Finally, in chapter 5 we conclude our main ideas.

Chapter 2

Theoretical Aspects

2.1 Deformation of Nuclei

The usual shape of a nucleus tends to be a sphere-like one, being completely spherical in the absence of interactions between the valence nucleons (equilibrium shape), which is the case for closed-shell nuclei, also known as magic nuclei.

In the most general case, one could parameterize the nuclear surface as a expansion in spherical harmonics $Y_{\lambda,\mu}$ [10], given by the expression

$$R(\theta,\varphi) = R_0 \left(1 + \sum_{\lambda=2}^{\lambda_{\max}} \sum_{\mu=-\lambda}^{\lambda} \alpha_{\lambda,\mu} Y^*_{\lambda,\mu}(\theta,\varphi)\right) , \tag{2.1.1}$$

where $R_0 \approx 1.2A^{1/3}$ is the (spherical) nuclear radius and $\alpha_{\lambda,\mu}$ being the deformation parameters. We can observe in the expression that the sum considers multipole terms from $\lambda = 2$ onwards, disregarding dipole deformations ($\lambda = 1$). The reason for this, as discussed in Ref. [11], is because the dipole deformations account for a shift of the center of mass of the nucleus rather than to a proper deformation.

Taking into account the fact that the radius must be a real quantity, another condition is imposed [12],

$$(\alpha_{\lambda,\mu})^* = (-1)^{\mu} \alpha_{\lambda,-\mu} , \tag{2.1.2}$$

therefore reducing the number of free parameters.

For the particular case in which the shape of the nucleus is symmetric with respect of a given axis, that is usually taken as the z axis, all parameters with $\mu \neq 0$ will vanish, so we can call the remaining parameters as $\beta_\lambda = \alpha_{\lambda,0}$, and we rewrite the expression for the radius as

$$R(\theta, \varphi) = R_0 \left(1 + \sum_{\lambda=2}^{\lambda_{\max}} \beta_\lambda Y^*_{\lambda,0}(\theta, \varphi) \right) . \tag{2.1.3}$$

Each of the β_λ parameters is associated with a different type of deformation of the nucleus, like the quadrupole shapes ($\lambda = 2$) and octupole shapes ($\lambda = 3$). Both of them are of interest for our work, in particular the last one, as there are more open questions related to its presence in different regions of the periodic table. It is important to mention that deformations with $\lambda > 4$ do exists, although they do not seem to be of importance for the study of nuclear structure [11].

The different types of deformation have their microscopic origin in the attempts of the nuclear system of minimizing its total energy [2], and arise from different configurations in the number of protons, Z, and neutrons, N.

2.1.1 Rotational deformation

Following the discussion made in Refs. [10] and [13], let us consider the principal axes from the nucleus to be labeled as 1, 2 and 3, with 3 being the symmetry axis. These axes form an intrinsic frame of reference, that rotates along with the nucleus with angular velocity ω. We can separate the hamiltonian of the system in two parts, a intrinsic part that is dependent of the intrinsic variables of the system, namely (q_i, p_i), and a rotational part, dependent on the angular momenta L_ω and possibly, other quantum numbers, that we will label by a, this is,

$$H_{\text{nucleus}} = H_{\text{int}}(q_i, p_i) + H_{\text{rot},a}(L_\omega) . \tag{2.1.4}$$

Therefore, the eigenstates of the hamiltonian will be a product of two states depending on each variable, namely,

$$\Psi_{a,L} = \Phi_a(q, p)\varphi_{a,L}(\omega) . \tag{2.1.5}$$

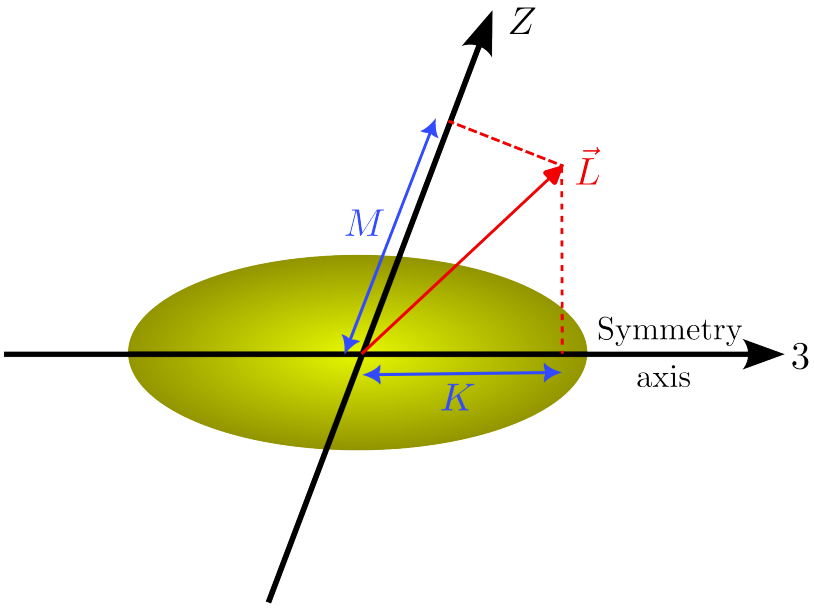

Figure 2.1.1: Orientation of the intrinsic and laboratory frames in an axially symmetric nucleus. Here, K represents the proyection of the angular momentum L on the symmetry axis, and M represents the proyection over the z axis of the laboratory frame.

Let us discuss first the rotational hamiltonian. Clasically, the angular momentum of a rotating object is given by

$$\mathbf{L} = I\boldsymbol{\omega}\,, \tag{2.1.6}$$

where I is the moment of inertia of the object. If we consider the object to have axial symmetry about 3, then we have that the diagonal components of the inertia tensor in the intrinsic frame satisfy $I_1 = I_2 = I$, and I_3 is a constant of the motion. Then, after quantization, a hamiltonian for the rotating system can be given by (Ref. [10])

$$H = \frac{\hbar^2}{2I}(L^2 - L_3^2) + \frac{\hbar^2}{2I_3}L_3^2\,. \tag{2.1.7}$$

If we label as K the eigenvalues of L_3 and by M the eigenvalues of L_z, that is, the projection of the angular momentum on the z axis of a Laboratory Frame with coordinates (x, y, z) (see Fig. 2.1.1 for a visualization of the reference frames), and $L(L+1)$ the eigenvalues of L^2, then we can completely define a state of motion of the nucleus, analogous with the procedure with the classical Euler angles.

The eigenvalues of the hamiltonian (2.1.7) are therefore given by

$$E_{\text{rot}} = \frac{\hbar^2}{2I}(L(L+1) - K^2) + \frac{\hbar^2}{2I_3}K^2 \,. \tag{2.1.8}$$

From now onwards, we will occupy ourselves only with systems with $K = 0$, as the work made during this thesis is restricted to states in the groundstate band for positive parity ($K^\pi = 0^+$), and as stated in Ref. [1], in the light actinides, like Radium, the lowest lying negative parity band is the band with $K^\pi = 0^-$. Then, the rotational wavefunction for a system might be

$$\varphi_{L,K=0,M}(\omega) = \frac{1}{\sqrt{2\pi}} Y_{L,M}(\theta, \phi) \,. \tag{2.1.9}$$

Given that our Hamiltonian does not depend on the position in the intrinsic frame, it is invariant under a rotation of 180° around one of the axes perpendicular to the symmetry axis, like the 2 axis, we can say that the system is $\mathscr{R}$ invariant, with the $\mathscr{R} = \mathscr{R}_2(\pi)$ operator acting on the intrinsic frame. Thus, this rotation $\mathscr{R}$ is part of the intrinsic degrees of freedom of our nucleus, and not of the rotational degrees of freedom. This condition can be expressed, as stated in [13], as

$$\mathscr{R}_c^{\text{ext}} = \mathscr{R}_i \,, \tag{2.1.10}$$

where $\mathscr{R}^{\text{ext}}$ represents a rotation acting on the external variables, the possible values of c are x, y, z, the axes of the the laboratory frame, and $i = 1, 2, 3$.

These eigenstates can be labeled by the eigenvalues of $\mathscr{R}$, that we shall represent as r. On the intrinsic part of our wavefunction, we have that

$$\mathscr{R}_i^2 \Phi_{r,K=0}(q) = r^2 \Phi_{r,K=0}(q) = \Phi_{r,K=0}(q) \,, \tag{2.1.11}$$

as $\mathscr{R}^2 = \mathscr{R}_2(2\pi)$ when the angular momentum of the system is of integer value, and therefore, $r = \pm 1$.

On the other hand, when working on the laboratory frame, we will have that the rotation $\mathscr{R}_c$ inverts the direction of the symmetry axis, that is, $(\theta \to \pi - \theta, \phi \to \phi + \pi)$, so when acting over the external wavefunction, we have that

$$\mathscr{R}_c Y_{L,M}(\theta, \phi) = (-1)^L Y_{L,M}(\theta, \phi) \,, \tag{2.1.12}$$

from where we observe that $r = (-1)^L$, and therefore, the rotational spectrum will contain states with only even or only odd values of L.

On the other hand, the parity operator $\mathscr{P}$ on the intrinsic basis $(1, 2, 3)$ acts over the intrinsic wavefunction as

$$\mathscr{P}\Phi_{K=0}(q) = \pi\Phi_{K=0}(q)\,, \tag{2.1.13}$$

such that its eigenvalues are $\pi = \pm 1$, so every member of the band will have the same parity. Note that, given the fact that the value of r emerges from the rotational wavefunction, the quantum numbers π and r are independent from each other.

Finally, if our hamiltonian possesses $\mathscr{T}$ invariance, that is, invariance under time reversal ($t \to -t$), and it is also $\mathscr{R}$ invariant, then we can choose the phases for the intrinsic states such that the combination $\mathscr{R}\mathscr{T} = 1$, in which case it acts on the intrinsic wavefunction as

$$\mathscr{T}\Phi_{K=0}(q) = r\Phi_{K=0}(q)\,, \tag{2.1.14}$$

and as its action over the spherical harmonics is given by

$$\mathscr{T}Y_{L,M}(\theta,\phi) = (-1)^M Y_{L,-M}(\theta,\phi)\,, \tag{2.1.15}$$

its action over the total wavefunction is

$$\mathscr{T}\Psi_{K=0,L,M} = (-1)^{L+M}\Psi_{K=0,L,-M}\,. \tag{2.1.16}$$

With these symmetries into consideration, different geometries can be observed in nuclei, particularly quadrupole deformation, which originates from a system which hamiltonian has $\mathscr{R}-$, $\mathscr{P}-$ and $\mathscr{T}$-symmetries, in which its hamiltonian possesses $\mathscr{R}\mathscr{P}$- and $\mathscr{T}$-symmetries, but not $\mathscr{R}$- and $\mathscr{P}$-symmetry.

Given that the discussion will focus on states with $K = 0$, the rotational energy in equation (2.1.8) becomes

$$E_{\text{rot}} = \frac{\hbar^2}{2I}L(L+1)\,, \tag{2.1.17}$$

where the moment of inertia is defined as

$$I_\kappa = \frac{\hbar L_\kappa}{\omega_\kappa}\,, \tag{2.1.18}$$

and where κ is an index for the different components of the vector operators, and the angular frequency ω can also be obtained from a power series expansion via the relation

$$\hbar^2 L(L+1) = \omega^2 I^2\,. \tag{2.1.19}$$

2.1.2 Vibrational deformation

The existence of spherical shapes in the presence of magic nuclei, as well as the existence of shapes with permanent deformation previously discussed, suggest the existence of intermediate shapes, that are interpreted as fluctuations or vibrations between the spherical shape and the deformed one.

One could approximate the vibrations on the nuclear surface as an harmonic oscillator which, in the second quantization formulation, is described with a hamiltonian of the form

$$\hat{H} = \hbar \sum_k \omega_k \left(\hat{A}_k^\dagger \hat{A}_k + \frac{1}{2} \right)\,, \tag{2.1.20}$$

where $\hat{A}_k$ and $\hat{A}_k^\dagger$ are the anihilation and creation operators for a phonon, and where they satisfy $[\hat{A}_k, \hat{A}_k^\dagger] = 1$, and each k represents a vibrational mode. This approximation supposes a spherical equilibrium shape. This hamiltonian has the following eigenvalues,

$$E_n = E_0 + \hbar \sum_k \omega_k n_k\,, \tag{2.1.21}$$

where E_0 is the groundstate energy and n_k is the number of phonons of a mode with k units of angular momentum and parity $(-1)^k$. In nuclear structure, it is common to fix the groundstate to an energy of zero, so the energy spectra will read

$$E_n = \hbar \sum_k \omega_k n_k\,. \tag{2.1.22}$$

If one adds a phonon with a given k, it is equivalent to add a Y_{km} dependence on the nuclear wavefunction [14]. When adding more phonons, the number of

possible states will be fully determined when considering the symmetrization or antisymmetrization of the total wavefunction. One example of this, in the case of even-even nuclei, will be developed in more detail in the next subsection.

The previously described procedure is adequate in the regime used in this work, although it should be mentioned that for states with sufficiently large values of angular momentum, the equilibrium shape could become non-spherical [13], and the spectra will not exhibit the constant separation between states that can be deduced from this hamiltonian.

Before entering on the next subsections of the discussion, we must clarify that, when we refer to an $E\lambda$ or $B(E\lambda)$ transition, we refer to transitions occurring between states with a difference in angular momentum of λ between them, for example, between the state L and the state $L - \lambda$.

2.1.3 Quadrupole deformation

The existence of large $B(E2)$ values that could not be explained by the predictions of the Shell Model was the first evidence for the existence of deformation in nuclei, and were explained as having their origin in rotational degrees of freedom, giving birth to a collective model of nuclear structure [13]. The geometry of nuclei with this deformation is that of a spheroid that may be oblate or prolate, depending on the value of the parameter β_2.

For even-even nuclei, the low-energy spectra shows the sequence of states $L^\pi = 0^+, 2^+, 4^+, \ldots$ with energies following roughly the equation of a symmetric rotor, that is, equation (2.1.17).

This spectra, and thus nuclei with permanent quadrupole deformation, can be observed in regions mid-way of a closed shell, with many particles outside of them. A typical way of conveying this information is defining the ratio $R_{4/2}$ between the energy of the 4^+ state and the energy of the 2^+ state. For permanent deformation, via the values obtained by equation (2.1.17), one gets thar $R_{4/2} = 20/6 \approx 3.33$. The levels that satisfy this expression for the energies form what is called a rotational band.

Via an analysis of the energy spectra, more evidence of the presence of quadrupole deformation can be found. Firstly, the fact that the low-lying spectra does not

possess states with odd values of angular momentum is a consequence of the $\mathscr{R}$ symmetry of the system, the absence of states with odd parity in the rotational band is a consequence of the $\mathscr{P}$ invariance of the intrinsic hamiltonian, and finally the absence of doublets with the same angular momentum and parity is a consequence of the $\mathscr{T}$ invariance of the intrinsic hamiltonian, according to Ref. [13]. The presence of these three invariances is, as stated previously in this chapter, clear evidence of an spheroidal shape.

In the case of quadrupole vibrations, the first evidence is again obtained via the ratio between the two first excited states, $R_{4/2}$. For this, we may first explain the presence of different values of angular momentum and their origin from the number of quadrupole phonons in them, that is, phonons with $k = 2$ and parity $(-1)^2 = +1$. If one adds one quadrupole phonon to the groundstate of an even-even nuclei, which is always 0^+, one obtains a 2^+ state. Adding a second quadrupole phonon introduces not only a 4^+ state, but also a second 0^+ and 2^+ states, the three of them with similar energies. This triplet of states emerges from the possible configurations of the M components of the spherical harmonics associated with each phonon. Given that the total angular momentum added to the groundstate is $L = 4$, then the possible $M = M_1 + M_2$ values go from -4 to $+4$, and the possible combinations are given in table 2.1.1.

	M_1				
M_2	-2	-1	0	$+1$	$+2$
-2	-4	-3	-2	-1	0
-1	-3	-2	-1	0	$+1$
0	-2	-1	0	$+1$	$+2$
$+1$	-1	0	$+1$	$+2$	$+3$
$+2$	0	$+1$	$+2$	$+3$	$+4$

Table 2.1.1: Possible combinations of the z projections, M_1 and M_2, of two quadrupole phonons into the total z component M. Table adapted from Ref. [14].

Nonetheless, given that for an even-even nuclei, the total wavefunction must be totally symmetrical, configurations like $(M_1 = +1, M_2 = -2)$ and $(M_1 = -2, M_2 = +1)$ must be identical, so there are only 15 possible combinations, those being one with $M = -4$, one with $M = -3$, two with $M = -2$, two with $M = -1$, three with $M = 0$, two with $M = +1$, two with $M = +2$, one with $M = +3$ and one with $M = +4$. Then, we can observe that the possible values of L that admits all these configurations are $L = 4$ for $M \in \{-4, -3, -2, -1, 0, +1, +2, +3, +4\}$,

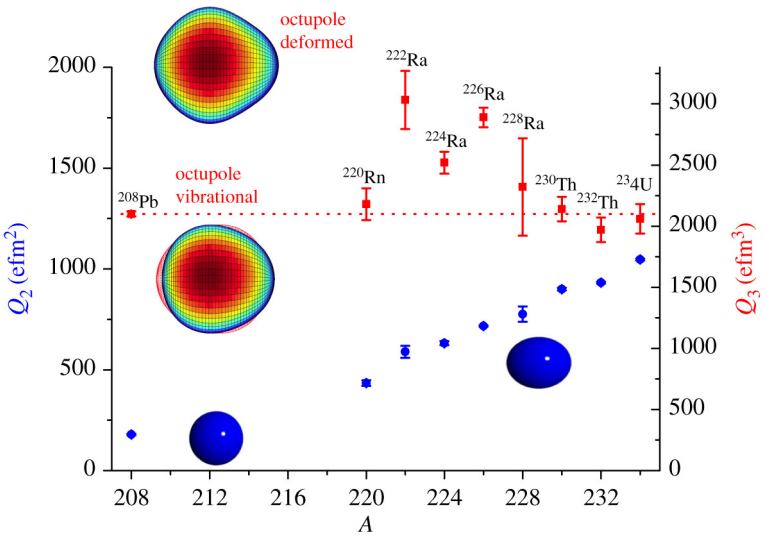

Figure 2.1.2: The systematics of measured $E2$ and $E3$ intrinsic moments Q_λ for $0^+ \to 2^+$ and $0^+ \to 3^-$ transitions, respectively, in the heavy mass region ($A \geq 208$). Figure taken from Ref. [6], published under the CC-BY-4.0 license.

$L = 2$ for $M \in \{-2, -1, 0, +1, +2\}$, and $L = 0$ to account for the third $M = 0$. A similar analysis can explain the following values of angular momentum in a vibrational spectra.

As we are interested only in the groundstate band, the only value of the triplet that is of interest for us is the 4^+ state, which is related to a two phonon state with energy $E(4^+) = E(n_2 = 2) = 2\hbar\omega_2$, while the 2^+ state is related to a one phonon state with $E(2^+) = E(n_2 = 1) = \hbar\omega_2$. Therefore, the charasteristic ratio $R_{4/2}$ between these states is equal to 2, and the states in the groundstate band will be evenly spaced.

Regarding the enhanced $E2$ transitions, we can observe in figure 2.1.2 the values of the intrinsic quadrupole moments, $Q_2 \sim \sqrt{B(E2)}$ (in blue), that for ^{208}Pb, a double magic nuclei and therefore with two closed shells, the moment is quite low in comparison with the ones observed in nuclei far from the closed shell, and actually the value of Q_2 increases when the number of nucleons, A, increases.

These deformations can be studied with different models that have different approaches, like the Shell Model, microscopic models, collective models, mean-field calculations and, in our interest, algebraic models. A first approach from an algebraic model to describe a quadrupole deformed system is the Elliott SU(3) model [15], in which the hamiltonian of the system possesses an harmonic oscillator

term to account for shape oscillations, and one interaction term, given by the quadrupole-quadrupole interaction, accounting for the permanent deformation. Then, the hamiltonian may be written as,

$$H = H_0 - \frac{1}{2}\kappa \sum_q Q^\dagger_{2q} Q_{2q} \,, \tag{2.1.23}$$

where H_0 corresponds to the harmonic oscillator hamiltonian. One of the strengths of this model is the fact that we could assume that the transition operator that describes $E2$ transitions is proportional to the quadrupole interaction Q_{2q}, reinforcing this quantity as a clear evidence of quadrupole deformation.

2.1.4 Octupole deformation

The presence of negative parity states in the low-lying energy spectra of some nuclei, observed early in the history of nuclear physics, led to the suggestion that there should be deformed nuclei with a reflection asymmetric shape [12], following the discussion previously made in this document, as symmetric shapes like the quadrupole ones do not allow the presence of states with different parity.

The regions in which this deformation is stronger is when both Z and N are just higher than the magic numbers, this is, $Z, N \sim 34, 56, 88, 134$ [1], like the lanthanide region, where $Z \sim 56$ and $N \sim 88$, and the actinides where $Z \sim 88$ and $N \sim 134$. The geometry of these nuclei is usually refered to as a pear shape, which is a consequence of the loss of the $\mathscr{R}$ symmetry of the system. This can be viewed in the presence of states with both odd and even values of angular momenta in the low-lying energy spectra, while we could also observe a violation of $\mathscr{P}$ parity from the fact that in octupole deformed nuclei, the groundstate band presents a parity alternating behavior. However, this shapes preserve the so called $\mathscr{R}\mathscr{P}$ symmetry, represented by the operator $\mathscr{S} = \mathscr{P}\mathscr{R}^{-1}$. Geometrically, this represents a reflection in a plane that contains the symmetry axis [15]. This $\mathscr{S}$ operator has its eigenvalues represented by the simplex quantum number s, corresponding to the product between the eigenvalues of $\mathscr{R}$ and $\mathscr{P}$,

$$s = \pi(-1)^L \,. \tag{2.1.24}$$

This symmetry is the reason of the parity-alternating rotational spectra observed

in these kinds of even-even nuclei. These alternating parities could have the following structure, depending on the value of s,

$$L^{\pi} = 0^{+}, 1^{-}, 2^{+}, \dots , \; s = +1 \,, \tag{2.1.25}$$

$$L^{\pi} = 0^{-}, 1^{+}, 2^{-}, \dots , \; s = -1 \,. \tag{2.1.26}$$

One of the first experimental evidence for the existence of octupole shapes emerges from the observation of enhanced $E1$ and $E3$ transitions. According to Ref. [6], the first ones seem to be enhanced from the new charge distribution that occurs inside the nucleus, focusing them in the more pointed end of the "pear", although the interaction between the individual nucleons might reduce significantly the collective enhancement, giving a near-zero value for the $B(E1)$ transitions. Then, to study the behavior of the $B(E3)$ transitions is more reliable, since they have a more collective origin and are not affected by the individual interactions [1, 6].

In figure 2.1.2 the values of the Q_3 intrinsic moments, derived from the $B(E3)$ transitions, with $Q_3 \sim \sqrt{B(E3)}$, are shown for the region of heavy nuclei. It can be seen that for ^{222}Ra, ^{224}Ra and ^{226}Ra there is an enhancement on the values of Q_3 in comparison with their neighbors, which is evidence of a rotational deformation, in contrast to the behavior of the other nuclei shown, that is consistent with the behavior of an octupole vibrator [1].

Regarding the analysis of the energy spectra, the very low-lying 1^{-} states in some nuclei suggest the presence of stable octupole deformation [16]. In this case, the energy spectra of the positive and negative parity states is given, from a given value of L onwards (usually $L \sim 5$), from the energy of a quantum rotor like equation (2.1.17), as stated in Ref. [2]. The angular momenta of the positive and negative parity states will in these cases be equal to the vector that describes the rotation of the nucleus, R, conventionally aligned to the x axis.

Vibrational deformation, on the other hand, usually appears as octupole modes of a quadrupole deformed equilibrium shape, having their origin in the presence of an octupole phonon that we may call n_3, which carries 3 units of angular momentum, coupled to the rotation vector, so the angular momentum of the negative parity states is given by $L^{-} = R + n_3$.

One way that one might study this approach is via the so called rotational

alignment of the nucleus, where one studies the behavior of the quantity $\Delta i_x = L^- - L^+$ versus the rotational frequency of the nucleus, that is approximately given by $\hbar\omega \approx (E_L - E_{L-2})/2$, being E_L the energy of a state with given L. If the nuclei has rotational deformation then the expected value of Δi_x is zero, as in this case $L^+ = L^- = R$. On the other hand, for octupole vibrational nuclei the expected value of Δi_x would be the angular momentum of the octupole phonon, $3\hbar$, as $L^- = R + 3\hbar = L^+ + 3\hbar$.

As with the quadrupole deformation, a microscopic approach can be made for higher multipoles in a sort of extension of the SU(3) model previously discussed, such that

$$H = \sum_j e_j c_j^\dagger c_{j'} - \frac{1}{2}\sum_\lambda \kappa_\lambda \sum_{\mu=-\lambda}^{+\lambda} Q_{\lambda\mu}^\dagger \cdot Q_{\lambda\mu} + H_{\text{pair}}\,, \tag{2.1.27}$$

where the first term corresponds to the shell-model potential (like an harmonic oscillator), the second correspond to the different multipole-multipole interactions, that for our purposes, can be limited to $\lambda = 3$, and the last one is the pairing hamiltonian, as stated in Ref. [1].

2.2 The Interacting Boson Model

The Interacting Boson Model (IBM) takes the notion given by the Shell Model that nuclei are composed by different states. In the shell model these states use to be grouped in shells, which are named "closed" when the maximum occupancy of their different states is reached. If it is not the case, there are so called valence nucleons, which are fermions, in the "unclosed" shells. The IBM instead considers nuclei composed by bosons, which are the counterpart of pairs of nucleons coupled to a good value of angular momentum [17].

Using the algebraic properties of the model, it is capable of describing the phenomena of low-lying collective states of medium-mass and heavy nuclei, such as the energy spectrum and the electromagnetic transition rates between states. Different extensions of this model have been developed for describing different types of phenomena in given regions of the nuclear chart, taking into account different physical considerations, but in this work we will discuss three of them: the so called *sd*-IBM-1, which consists of the original formulation of the model using bosons of positive parity and angular momenta $L^\pi = 0^+, 2^+$, the *sdf*-IBM-1,

that introduces the possibility to describe negative parity states using in addition bosons with angular momentum and parity $L^\pi = 3^-$, and the *spdf*-IBM-1, the one used in the calculations made in this work which also uses bosons with negative parity and angular momentum $L^\pi = 1^-$.

2.2.1 *sd*-IBM-1

As stated before, this model has its foundations in the hypotesis that the nucleus is a system made up by bosons, which correspond to nucleon pairs, without taking into account if these pairs are made up by protons or by neutrons. Specifically, we consider that there are two types of bosons, the s boson, with angular momentum $L^\pi = 0^+$, and the d boson, with $L^\pi = 2^+$. These bosons allow us to describe the positive parity collective states with low-lying energy [18].

From the point of view of the second quantization, let us consider the boson creation and anihilation operators, such that we have

$$s^\dagger, \tilde{s}, d^\dagger_\mu, \tilde{d}_\mu\,, \quad \mu = \{\pm 2, \pm 1, 0\}\,, \tag{2.2.1}$$

where μ corresponds to the projection on the z axis of the angular momentum, $\tilde{s} = s$, and $\tilde{d}_\mu = (-1)^\mu d_{-\mu}$. This last definition is made so that the operators behave like spherical tensors of Racah. We can express these tensors in a more compact notation, namely b_α can be one of the set $\{s, d_{-2}, d_{-1}, d_0, d_1, d_2\}$, where $\alpha = 1, 2, \ldots, 6$, so that they satisfy the boson conmutation relations given by

$$[b_\alpha, b^\dagger_\beta] = \delta_{\alpha\beta}\,,\ [b_\alpha, b_\beta] = 0\,,\ [b^\dagger_\alpha, b^\dagger_\beta] = 0\,. \tag{2.2.2}$$

A general hamiltonian in this model can be written as

$$H = E_0 + \sum_{\alpha\beta} e_{\alpha\beta} b^\dagger_\alpha b_\beta + \frac{1}{2}\sum_{\alpha\beta\gamma\delta} u_{\alpha\beta\gamma\delta} b^\dagger_\alpha b^\dagger_\beta b_\gamma b_\delta\,, \tag{2.2.3}$$

where E_0 is a real quantity, $b^\dagger b$ represents one body contributions to the hamiltonian, and $b^\dagger b^\dagger bb$ represents two-body contributions. The presence of these interaction terms gives the model the name of interacting bosons. One can

also write this hamiltonian in terms of multipole operators, which then becomes

$$H = E'_0 + \varepsilon_d \hat{n}_d + c_1 \hat{L} \cdot \hat{L} + c_2 \hat{Q}^\chi \cdot \hat{Q}^\chi + c_3 \hat{U} \cdot \hat{U} + c_4 \hat{V} \cdot \hat{V} \,, \tag{2.2.4}$$

where

$$\begin{aligned} \hat{n}_d &= d^\dagger \cdot \tilde{d} \,, \\ \hat{L} &= \sqrt{10}[d^\dagger \times \tilde{d}]^{(1)} \,, \\ \hat{Q}^\chi &= [d^\dagger \times \tilde{s} + s^\dagger \times \tilde{d}]^{(2)} + \chi[d^\dagger \times \tilde{d}]^{(2)} \,, \\ \hat{U} &= [d^\dagger \times \tilde{d}]^{(3)} \,, \\ \hat{V} &= [d^\dagger \times \tilde{d}]^{(4)} \end{aligned} \tag{2.2.5}$$

are the above mentioned multipole operators. In particular, $\hat{n}_d$ corresponds to the number operator for d bosons, $\hat{L}$ corresponds to the angular momentum operator, and $\hat{Q}^\chi$ corresponds to the quadrupole operator. The term $\hat{n}_s = s^\dagger \cdot \tilde{s}$ is not explicitely included in this realization, as it contributes to the E'_0 value.

This parametrization is interesting because it allow us to describe electromagnetic transitions between different states with transition operators proportional to each multipole term, those being

$$\begin{aligned} \hat{T}^{(E0)} &= \gamma'_0 + \beta''_0 \hat{n}_d \,, \\ \hat{T}^{(M1)} &= g' \hat{L} \,, \\ \hat{T}^{(E2)} &= \alpha_2 \hat{Q}^\chi \,, \\ \hat{T}^{(M3)} &= \beta_3 \hat{U} \,, \\ \hat{T}^{(E4)} &= \beta_4 \hat{V} \,. \end{aligned} \tag{2.2.6}$$

It is important to observe that on this version of the model there can only exist electric transitions of even order, and magnetic transitions of odd order.

Generally, we would need to solve the eigenvalue problem numerically for a given nucleus. However, there are three special cases in the context of the *sd*-IBM-1 that make use of group theory to give an analytical solution to the problem, being called dynamical symmetries.

Following Ref. [19], we can define a new set of operators $g : G_{\alpha\beta} = b^\dagger_\alpha b_\beta$, with

$\alpha, \beta = 1, \ldots, 6$. They satisfy the commutation relation

$$[G_{\alpha\beta}, G_{\rho\sigma}] = G_{\alpha\sigma}\delta_{\beta\rho} - G_{\rho\beta}\delta_{\sigma\alpha}\,, \tag{2.2.7}$$

along with the Jacobi identity, so they form a Lie Algebra. In fact, these operators satisfy the relations of the unitary Lie algebra $u(6)$, and are generators of the Lie group $U(6)$[1].

The $u(6)$ algebra has various sub-algebras, but in the context of nuclear physics we need to include the algebra of three-dimensional rotations, $so(3)$, if we want to describe systems with good values of angular momentum. With this condition, we have three sub-algebras that may be reduced to $so(3)$[2], that we denote by the group chains

$$\begin{aligned} &U(6) \subset U(5) \subset O(5) \subset O(3)\,, && \text{(I)} \\ &U(6) \subset SU(3) \subset O(3)\,, && \text{(II)} \\ &U(6) \subset O(6) \subset O(5) \subset O(3)\,. && \text{(III)} \end{aligned} \tag{2.2.8}$$

Geometrically, chain (I) represents spherical nuclei, chain (II) represents quadrupole-deformed nuclei, and chain (III) represents $\gamma-$unstable nuclei which do not present axial symmetry.

For the study of quadrupole-deformed nuclei, an appropiate hamiltonian is given by

$$H_{SU(3)} = E_0 - \kappa' \hat{L}\cdot\hat{L} - \kappa_2 \hat{Q}\cdot\hat{Q}\,, \tag{2.2.9}$$

but if we want to describe a given set of nuclei where a shape transition may occur, specifically from the $U(5)$ limit to the $SU(3)$ limit (from a spherical shape to a quadrupole-deformed one), according to Ref. [20] we can consider the following hamiltonian

$$H = E_0 + \varepsilon_d \hat{n}_d - \kappa' \hat{L}\cdot\hat{L} - \kappa_2 \hat{Q}\cdot\hat{Q}\,. \tag{2.2.10}$$

Nonetheless, as stated in Ref. [21], the term proportional to the angular momentum just renormalizes the moment of inertia of the nuclear system, and choosing $E_0 = 0$, we can simplify our Hamiltonian to

$$H = \varepsilon_d \hat{n}_d - \kappa_2 \hat{Q}\cdot\hat{Q} \tag{2.2.11}$$

[1] Note that the algebra is denoted in lowercase, while the group is denoted in uppercase.
[2] In the context of nuclear physics, all orthogonal groups that we may use are special, so we will drop the S onwards when refering to special orthogonal groups.

for the study of an isotopic chain.

Despite the success that this model has shown in the description of nuclei with quadrupole shapes, it is not capable of describing features of nuclei with negative parity states, which would involve the inclusion of negative parity bosons, as discussed in Ref. [22].

2.2.2 *sdf*-IBM-1

Given the experimental evidence about octupole features in the actinide region, Refs. [20, 23, 24] discussed that they may be described via an f boson, carrying a value of angular momentum $L^\pi = 3^-$, with a hamiltonian of the type

$$H = H_{sd} + H_f + V_{fd}\,, \tag{2.2.12}$$

where H_{sd} is the hamiltonian (2.2.3) describing the quadrupole mode, H_f describing the octupole mode, and V_{fd} describing the octupole-quadrupole interaction. In their first article about the subject, the authors introduced both the s boson of the $sd-$IBM, as well a s_f boson for the ground level of octupole excitations [23]. In the following works, however, they decided to identify this s_f boson with the s boson of the $sd-$IBM, which would be used in their work onwards.

In this case, analytical solutions are only found when working in the case of $n_f = 1$, this is, the case of octupole vibrations [25], reducing the full hamiltonian (2.2.12) to the expression

$$\begin{aligned} H = H_{sd} + \varepsilon'_f(f^\dagger \cdot \tilde{f}) + \sum_{L=0}^{4} x''_L[[f^\dagger \times \tilde{f}]^{(L)} \times [d^\dagger \times \tilde{d}]^{(L)}]_0^{(0)} \\ + w_2[[f^\dagger \times \tilde{f}]^{(2)} \times [d^\dagger \times \tilde{s} + s^\dagger \times \tilde{d}]^{(2)}]_0^{(0)}\,. \end{aligned} \tag{2.2.13}$$

The inclusion of the f boson allows to describe electromagnetic transitions that were previously forbidden, like the $E1$ and $E3$ transitions that, as discussed on the previous section, are clear evidence of octupole phenomena.

The algebraic structure of this model is given by the $U(13)$ group, via its decomposition in the tensor product $U_{sd}(6) \otimes U_f(7)$ as stated in Ref. [25], where $U_{sd}(6)$ is the algebra of the IBM-1 discussed in the previous section, and $U_f(7)$

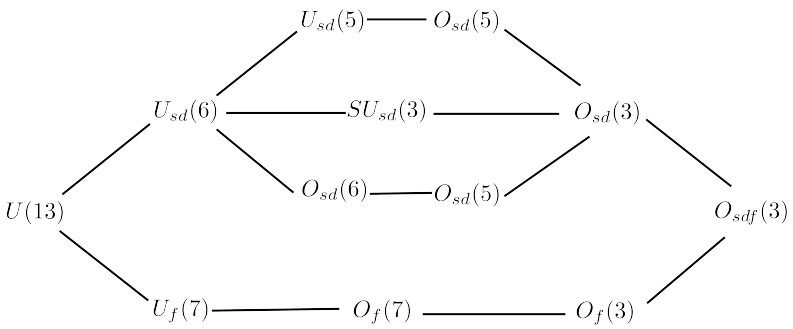

Figure 2.2.1: Dynamical symmetries associated to the decomposition of $U(13)$.

is the algebra generated by the operators $B_{\alpha\beta} = b^\dagger_\alpha \tilde{b}_\beta$, where $\alpha, \beta = 1, \ldots, 7$ and b_α corresponds to the f_μ operators with different projections of their angular momentum on the z axis. The detailed construction of this algebra is discussed in Ref. [26]. In figure 2.2.1 we present a diagram of the possible dynamical symmetries associated to this decomposition.

One particular case of interest for the discussion of our work is the one analyzed in Ref. [20], in which the authors describe nuclei that possess a transitional quadrupole shape between the $U(5)$ and $SU(3)$ limits, while also presenting octupole phenomena. They may, therefore, be described with a hamiltonian of the form

$$H = H_{sd}^{(I)\to(II)} + \epsilon_f + \theta_f N + z[Q_f^{(2)} \times Q^{(2)}]^{(0)}\,, \tag{2.2.14}$$

where $H_{sd}^{(I)\to(II)}$ corresponds to equation (2.2.10), $n_f = 1$, $Q_f^{(2)} = 2\sqrt{7}[f^\dagger \times \tilde{f}]^{(2)}$ is the quadrupole operator of the f boson, $Q^{(2)}$ is the sd quadrupole operator defined in equation (2.2.5), and θ_f and z are two parameters controlling the interaction between the octupole bosons and the s and d bosons.

This hamiltonian, while being able to reproduce the energy spectra and the $E3$ transitions with quite some success, fails to describe the experimentally observed $E1$ transitions without the need to include terms of higher order in the operator to calculate them.

More recently, there have been works with the sdf-IBM in combination with nuclear energy density functionals calculations in the lanthanide and actinide regions [27, 28], that do not limit the number of f bosons and use different

definitions of a general hamiltonian of the form

$$H = H_{sd} + H_f + H_{sdf} \,, \tag{2.2.15}$$

where H_{sd} is consistently defined as the hamiltonian of equation (2.2.10), H_f is the hamiltonian of the octupole mode, that usually includes the f boson number operator and a quadrupole f boson interaction Q_f, and H_{sdf} is the hamiltonian of the interaction between the s, d and f bosons, usually involving a term of the type $Q_{sd} \cdot Q_f$. These works include modfications that allow a better description of the $E3$ transitions, as well as other phenomena, but they still lack a satisfactory description of $E1$ transitions.

2.2.3 *spdf*-IBM-1

The difficulties to describe $E1$ transitions with the *sdf*-IBM-1 suggested that the inclusion of another boson with negative parity may be needed. This new boson, carrying 1 units of angular momentum, is labeled as the p boson [29]. The inclusion of the p boson was not met without some doubts, as they could be associated with a dipole mode, that as discussed before, should only affect the position of the center of mass of the nuclei. However, according to Ref. [29], it facilitates the phenomenological treatement of the algebraic properties, and appears to have its origins in the underlying microscopic structure of the nucleus.

The inclusion of the p boson allows a better depiction of the $E1$ transitions, in contrast with the ones made in the context of the *sdf*$-$IBM-1, without the need to include aditional high order terms to the transition operator. In adition, Ref. [30] suggests that the inclusion of the p boson is justified since the interaction between quadrupole and octupole degrees of freedom produces correlated pairs of nucleons coupled to angular momentum $L^\pi = 1^-$, so the p boson is justified to simulate this behavior.

From a group theoretical point of view, this model is associated with the $u(16)$ algebra, and therefore, the $U(16)$ group, and a full discussion about the dynamical symmetries observed can be found in Refs. [31, 32].

A general hamiltonian that may be used in the context of this model is the one proposed by Ref. [30] for the study of thorium isotopes, that generalizes the hamiltonian shown in equation (2.2.11) to include the dipole and octupole

interactions, resulting in the form

$$H = \varepsilon_d n_d + \varepsilon_p n_p + \varepsilon_f n_f - \kappa_1 Q^{(1)} \cdot Q^{(1)} - \kappa_2 Q^{(2)} \cdot Q^{(2)} - \kappa_3 Q^{(3)} \cdot Q^{(3)} \,, \quad (2.2.16)$$

where the number operators for the negative parity bosons are, respectively, $n_p = -p^\dagger \cdot \tilde{p}$ and $n_f = -f^\dagger \cdot \tilde{f}$, and the $Q^{(2)}$ operator is consistently defined as

$$\begin{aligned} Q^{(2)} &= Q^{(2)}_{sd} + \alpha Q^{(2)}_{pf} \\ &= [d^\dagger \times \tilde{s} + s^\dagger \times \tilde{d}]^{(2)} + \chi_{dd}[d^\dagger \times \tilde{d}]^{(2)} \\ &\quad + \alpha \left(\chi_{pp}[p^\dagger \times \tilde{p}]^{(2)} + \chi_{ff}[f^\dagger \times f]^{(2)} + \chi_{pf}[p^\dagger \times \tilde{f} + f^\dagger \times \tilde{p}]^{(2)} \right) , \end{aligned} \quad (2.2.17)$$

where the α and χ parameters change in the literature, as also do the dipole and octupole operators. This study shows a great agreement between the theoretical calculations and the experimental data both for energies and electromagnetic transitions, specially the $E1$ moments with transition operators with only one body terms, consistent with the transition operators for $E2$ and $E3$.

In the same context, Ref. [21] uses a hamiltonian similar to equation (2.2.16), focusing only on the multipole terms. The authors derive the definition of the dipole and octupole operators from the $r^\lambda Y_{\lambda\mu}$ matrix elements between the *sd* shell ($N = 2$) and the *pf* shell ($N = 3$) harmonic oscillator major shells, in the context of the shell model. Here, N is the number that appears in the energy eigenvalues for an harmonic oscillator. Those derivations are made as the quadrupole operator is known to be derived from the same principle. The inclusion of the dipole term is again justified from its influence on the electromagnetic transitions.

Another hamiltonian that may be used in the context of the model is the one used in Ref. [9] in the actinide region, considering only the number operators and the quadrupole interaction presented in equation (2.2.17), that is

$$H = \varepsilon_d n_d + \varepsilon_p n_p + \varepsilon_f n_f - \kappa Q^{(2)} \cdot Q^{(2)} \,. \quad (2.2.18)$$

This selection is made given the diagonal nature of the terms in the decomposition $U_{spdf}(16) \supset U_{sd}(6) \otimes U_{pf}(10)$. This work presents good results for the $E1$ transitions with a one body operator, although it makes use of e_1 effective charges that vary along the isotopic chain to make precise fits. It also makes the point that to include negative parity bosons in the positive parity states, it is necessary to also include

a dipole interaction to the hamiltonian (2.2.18), although this inclusion does not allow to exploit the diagonal nature of the previously mentioned hamiltonian.

They also observe that in the case in which $\varepsilon_p = \varepsilon_f$ in the hamiltonian (2.2.18), then one dynamical symmetry of the system emerges, the one asociated with the rotational limit of the model that separately conserves the number of positive and negative parity bosons,

$$U_{spdf}(16) \supset U_{sd}(6) \otimes U_{pf}(10) \supset SU_{sd}(3) \otimes SU_{pf}(3) \supset SU_{spdf}(3) \supset O_{spdf}(3)\,. \tag{2.2.19}$$

During the last decade, there was a great boom in experimental data for the $E1$ and $E3$ transitions in different nuclei, like radon [4] and radium [5, 6], which were used by Ref. [8] in the context of the *spdf*-IBM-2, that differentiates bosons made up from protons of those made up from neutrons. The calculations of this work reproduced sucessfully the experimental data available for the energies, $E1$, $E2$ and $E3$ transitions on radon isotopes with a hamiltonian containing a small number of free parameters.

Chapter 3

Methods

As stated previously in this document, the objective of this work is to study the octupole phenomena in the even-even Radium isotopes in the framework of the *spdf*-IBM-1, aiming in particular to

1. Make numerical calculations to find a set of hamiltonian parameters for each nuclei in the $^{216-228}$Ra isotopic chain that is able to reproduce fairly well the experimental data available.
2. Identify the presence or absence of octupole deformation in the studied Radium isotopes.
3. Study the effects that the interaction terms in our hamiltonian have on the description of octupole-deformed nuclei.

For the present work, we have adopted a hamiltonian of the same form as the one used by Refs. [30, 33], given by

$$\hat{H} = \varepsilon_p \hat{n}_p + \varepsilon_d \hat{n}_d + \varepsilon_f \hat{n}_f - \kappa_1 \hat{Q}^{(1)} \cdot \hat{Q}^{(1)} - \kappa_2 \hat{Q}^{(2)} \cdot \hat{Q}^{(2)} - \kappa_3 \hat{Q}^{(3)} \cdot \hat{Q}^{(3)} \,. \quad (3.0.1)$$

This election is made because we hypothesize that this hamiltonian is capable of reproducing the quadrupole phenomena observed in transitional nuclei between the $SU(3)$ limit and the $U(5)$ limit, as it was discusssed in the previous chapter, as well as the octupole phenomena related with vibrational and rotational octupole deformation. The inclusion of the dipole operator allow us to better describe the electromagnetic transitions that occur in the range of isotopes to be studied,

specially the $E1$ transitions, as it is stated in Refs. [9, 21].

For the multipole operators, we chose the definitions proposed in Ref. [21], those being

$$\hat{Q}^{(1)}_{\mu} = \sqrt{8}(d^{\dagger}\tilde{p} - p^{\dagger}\tilde{d})^{(1)} + \sqrt{10}(s^{\dagger}\tilde{p} - p^{\dagger}\tilde{s})^{(1)} + \sqrt{42}(d^{\dagger}\tilde{f} - f^{\dagger}\tilde{d})^{(1)}\,, \tag{3.0.2}$$

$$\hat{Q}^{(2)}_{\mu} = (s^{\dagger}\tilde{d} + d^{\dagger}\tilde{s})^{(2)} + \chi_d(d^{\dagger}\tilde{d})^{(2)} - \frac{9\sqrt{3}}{10}(p^{\dagger}\tilde{p})^{(2)} - \frac{3\sqrt{7}}{5}(p^{\dagger}\tilde{f} + f^{\dagger}\tilde{p})^{(2)} - \frac{3\sqrt{42}}{10}(f^{\dagger}\tilde{f})^{(2)}\,, \tag{3.0.3}$$

$$\hat{Q}^{(3)}_{\mu} = 2(p^{\dagger}\tilde{d} - d^{\dagger}\tilde{p})^{(3)} + \sqrt{5}(f^{\dagger}\tilde{s} - s^{\dagger}\tilde{f})^{(3)} + \sqrt{6}(f^{\dagger}\tilde{d} - d^{\dagger}\tilde{f})^{(3)}\,. \tag{3.0.4}$$

The choice of these multipole operators was made as they allow us to use a Q-consistent formalism for the study of the electromagnetic transitions and the multipole moments given their hermiticity. Although the authors define the χ_d parameter with a fixed value, $\chi_d = -\sqrt{7}/2$, we decided to make it a free parameter, as the value of $-\sqrt{7}/2$ is related to the generator of the $SU(3)$ group, describing permanent quadrupole deformation, while some of the isotopes on the chain itself are not necessarily deformed. This choice was also made aiming to potentially improve the results for the $E2$ transition rates.

On the other hand, the isotopic chain $^{216-228}$Ra was chosen as the experimental data suggests the existence of octupole deformation in ^{222,224,226}Ra, so we could take these results as reference on our analysis, expanding it to the near nuclei in search of the same kind of behavior in them.

The data for the energies was available in Ref. [34], while the transition rates were retrieved from Ref. [5] for ^{224}Ra, Ref. [6] ^{222}Ra and ^{228}Ra, Ref. [16] for ^{226}Ra and Ref. [34] for ^{216}Ra and ^{218}Ra. We were not able to find experimental data for the transition rates to the groundstate in ^{216}Ra, which is consistent with the lack of data for the low-energy states of this nuclei, and no data for the transition rates was available for ^{220}Ra, although the data regarding the energies was available.

3.1 Numerical calculations

Our method consisted in obtaining the sparse matrices for each term of the hamiltonian and the required transition operators via the ArbModel computer

code [35]. Then a Python code constructs our hamiltonian as given in equation (3.0.1), where each one of the parameters ε_i, κ_i are free, and subject to a least squares minimization routine. This routine makes use of the iMinuit package [36], which is based on the MINUIT routine proposed in Ref. [37]. Here, the eigenvalues and eigenvectors problem is solved numerically in each iteration via the scipy.sparse Python pachage with the LOBPCG method. This allows us to calculate the energies and the transition rates of the states in the groundstate and the low-lying states of both parities. The work was made with sparse matrices, which reduce considerably the memory usage compared to the use of dense matrices.

The χ^2 function is defined as

$$\chi^2 = W_E \sum_i \frac{(E_i^{\text{theo}} - E_i^{\text{exp}})^2}{\Delta {E_i}^2} + \sum_\lambda W_{T(E\lambda)} \sum_j \frac{(T(E\lambda)_j^{\text{theo}} - T(E\lambda)_j^{\text{exp}})^2}{\Delta T(E\lambda)_j{}^2} , \quad (3.1.1)$$

with $\lambda = 1, 2, 3$. Here it can be seen that the χ^2 includes the energies, that are directly the eigenvalues of the hamiltonian, as well as the transition matrix elements $T(E\lambda)$, defined as

$$T(E\lambda; L_i \to L_f) = \langle L_f || e_\lambda Q^{(\lambda)} || L_i \rangle , \quad (3.1.2)$$

where L_i, L_f are the initial and final states, e_λ are the effective bosonic charges, kept constant for all the isotopic chain, and $\langle \cdot || M || \cdot \rangle$ represents reduced matrix elements (a more extense definition is made in the appendix A.2). The ArbModel code generates the transition matrices with the constants required to define the reduced matrix elements. For each term on the χ^2 function, we added the experimental error as a weight for each term. We also included the W_k functions, which act as a relative weight between the energies and the transition matrices to give more relevance to the last ones on the minimization.

3.2 Presence of octupole deformation

Once the parameters are obtained, we can calculate the theoretical energies and matrix elements, and use the last ones for the calculation of the electric transition

rates $B(E\lambda)$, defined as

$$B(E\lambda; L_i \to L_f) = \frac{1}{2L_i+1} T(E\lambda; L_i \to L_f)^2 \,, \tag{3.2.1}$$

as well as intrinsic multipole moments Q_λ, with special interest in the octupole moment Q_3. These quantities are given by

$$Q_\lambda(L_i \to L_f) = \frac{1}{(L_i 0 \lambda 0 | L_f 0)} \sqrt{\frac{16\pi}{2\lambda+1} \frac{1}{2L_i+1}} T(E\lambda; L_i \to L_f) \,, \tag{3.2.2}$$

where $(L_i 0 \lambda 0 | L_f 0)$ is a Clebsch-Gordan coefficient, and for the special case of $\lambda = 1$,

$$Q_1(L_i \to L_f) = \frac{1}{(L_i 010 | L_f 0)} \sqrt{\frac{4\pi}{3} \frac{1}{2L_i+1}} T(E1; L_i \to L_f) \,. \tag{3.2.3}$$

In both cases, we are using the definitions given in Ref. [6] and its Supplementary Material.

The presence of non-zero octupole moments are the main evidence of the presence of octupole deformation in this isotopic chain, and we will compare our theoretical calculations with the available experimental data of Refs. [5, 6].

3.3 Analysis of the effects of the multipole terms.

To understand the effect of each of the multipole terms over the description of the octupole degrees of freedom in this chain, we will study three differents scenarios for the interactions included in our hamiltonian, these being

1. $H_{\text{int}} = \hat{Q}^{(2)} \cdot \hat{Q}^{(2)}$,
2. $H_{\text{int}} = \hat{Q}^{(2)} \cdot \hat{Q}^{(2)} + \hat{Q}^{(1)} \cdot \hat{Q}^{(1)}$,
3. $H_{\text{int}} = \hat{Q}^{(2)} \cdot \hat{Q}^{(2)} + \hat{Q}^{(3)} \cdot \hat{Q}^{(3)}$,

with the objective of observing and discussing the role of the last two interactions in an accurate description of octupole phenomena.

This is made by comparing the results obtained in each case between themselves and with the result of the full hamiltonian (3.0.1) including, in principle, the three multipole interactions. For this, we set the different κ_i parameter zero, in function

of the desired interactions. The motivation for this study emerges from the fact that, for example, Ref. [9] does not include octupole interaction on its hamiltonian, which rises the question about the necessity (or absence) of its inclusion. Thus, one might expect to observe a greater κ_2 strength in nuclei far from the closed shell, like $^{222-228}$Ra, as these nuclei should be closer to a quadrupole deformed shape, this being the reason behind always including the quadrupole term.

Chapter 4

Analysis and Discussion

4.1 Parameters.

As discussed in the previous chapter, the calculations were made via a computer program developed for this work, which can be found in Ref. [38]. These calculations resulted in a set of hamiltonian parameters presented in table 4.1.1.

Isotope	ε_d	ε_p	ε_f	κ_2	κ_1	κ_3	χ_d
^{216}Ra	0.777	1.999	0.689	0.0169	0.0051	0.0000	-2.405
^{218}Ra	0.674	1.200	0.728	0.0140	0.0018	0.0000	-3.262
^{220}Ra	0.557	1.099	0.549	0.0260	0.0044	0.0000	-2.900
^{222}Ra	0.170	0.801	0.415	0.0284	0.0036	0.0000	-2.578
^{224}Ra	0.176	0.899	0.779	0.0300	0.0043	0.0000	-1.920
^{226}Ra	0.196	1.280	0.891	0.0282	0.0052	0.0000	-2.098
^{228}Ra	0.245	1.195	0.793	0.0173	0.0032	0.0000	-2.733

Table 4.1.1: Set of parameters obtained for each nuclei of the isotopic chain. The results for the ε_i and κ_i parameters are given in MeV, while the χ_d parameter is adimensional.

At first glance, it is interesting that the κ_3 parameter becomes zero for the whole chain, implying that the octupole interaction is not needed for the description of the octupole degrees of freedom. This will be discussed further in a future subsection.

As can be seen more clearly in Fig. 4.1.1, we can observe two distinct regions of parameters, specifically for κ_1, κ_2 and χ_d: the first region regards the lighter nuclei ($^{216-220}$Ra), while the second one regards the nuclei that have experimental

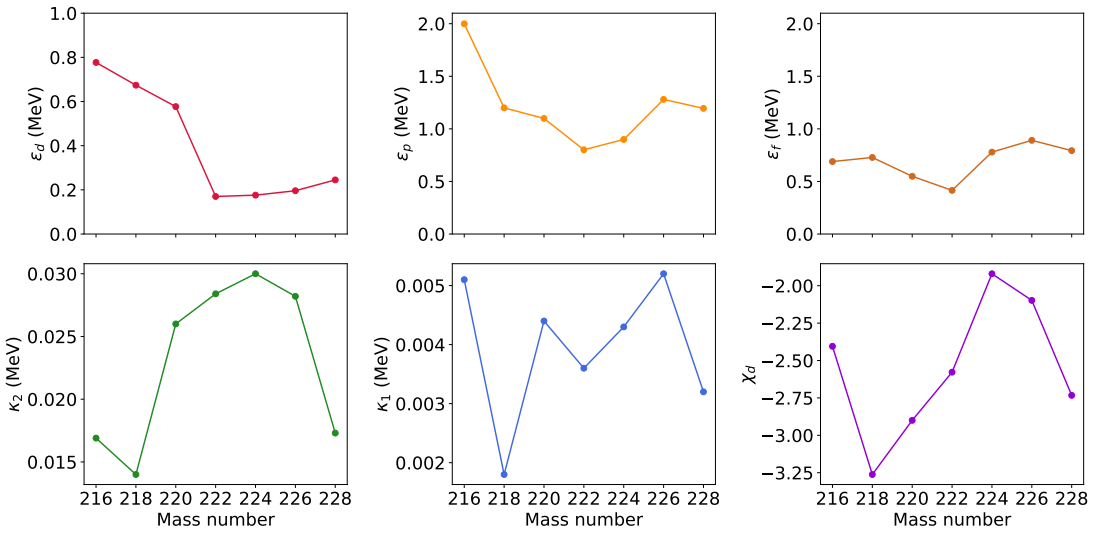

Figure 4.1.1: Evolution of the hamiltonian parameters as a function of the mass number.

evidence suggesting static and vibrational octupole deformation ($^{222-228}$Ra). This might also be related to the fact that the first isotopes mentioned possess a smaller set of experimental data available, mainly their energy spectra, possibly inducing to a behavior that does not follow the trend of the other nuclei of the chain. We can also observe that for the second region of parameters, the results satisfy that $\varepsilon_p > \varepsilon_f > \varepsilon_d$.

The energy of the quadrupole boson, ε_d, shows a rapid decrease with the mass number, minimizing at ^{222}Ra, and slowly increasing after. This might be attributed to the lowering of the energies of the states in the positive parity band as a consequence of the transition to a static quadrupole shape. The energy of the dipole boson ε_p has a behavior similar to a parabola, being consistent with the results in Ref. [9]. It can be observed that the nuclei for which ε_p and ε_f lie closer in energy is for ^{224}Ra, the nuclei which is understood to be the one where static octupole deformation is stronger.

4.2 Spectroscopic properties.

4.2.1 Energy Spectra

We present the results for the energy levels in the isotopic chain in figure 4.1.2. On the left side of each figure, we present the experimental energy levels retrieved

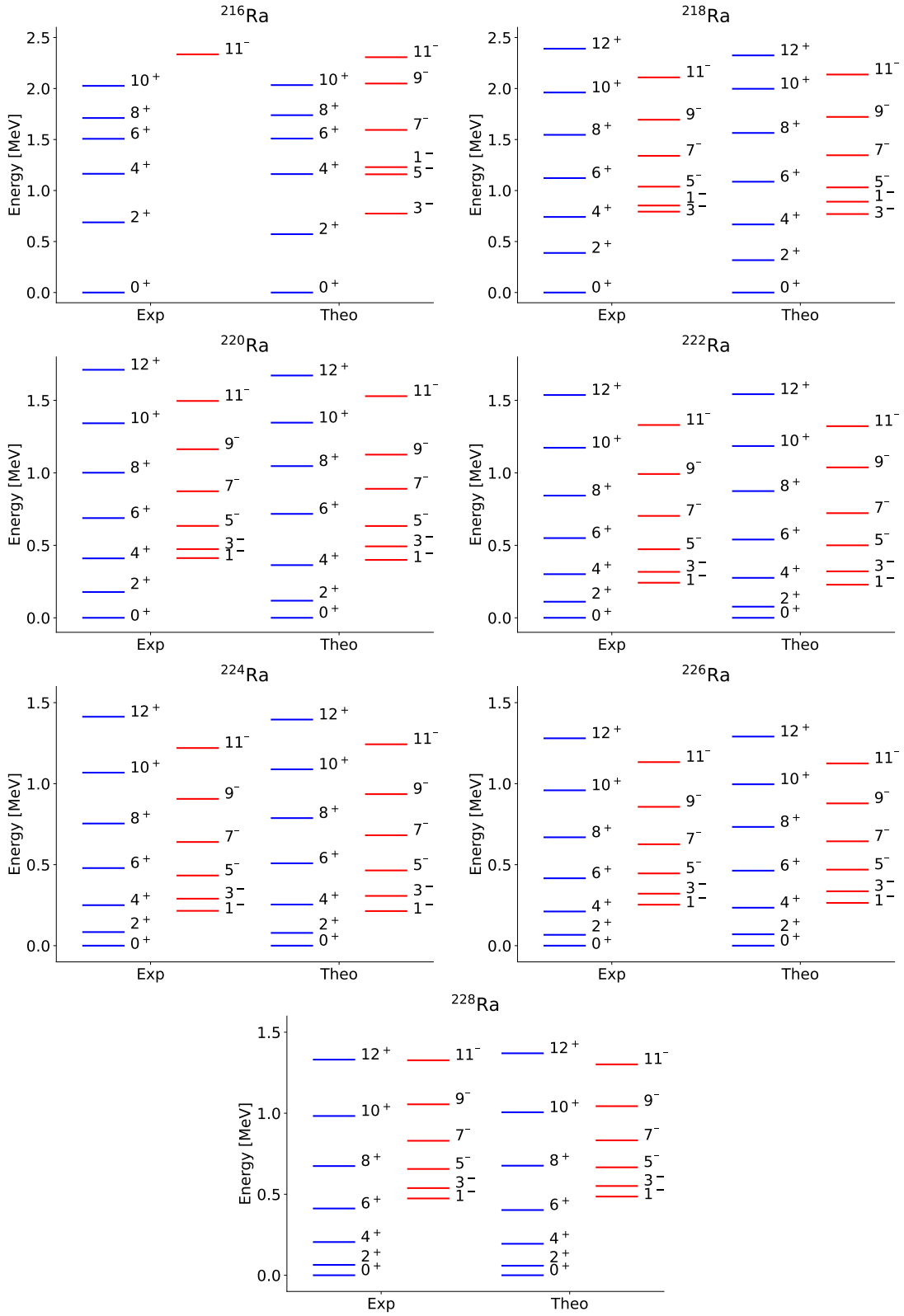

Figure 4.1.2: Experimental (left) and theoretical (right) energy spectra for $^{216-228}$Ra. The blue lines represent positive-parity states, while the red lines represent negative-parity states. The experimental results were obtained from Ref. [34].

from Ref. [34], while in the right side we present the results of our numerical calculations.

The model reproduces with quite great success the experimental results in all of the nuclei. The mean value of the Root Mean Squared Error (RMSE) for each nuclei is of 0.101 [MeV], with the highest RMSE being observed for ^{216,218}Ra, of around 0.15 [MeV]. These low values show that the model has great accuracy reproducing the experimental energy spectra for this chain, taking into consideration that we use only six parameters and twelve energy levels on the fitting process.

One might explain the strange behavior of the 1^- state in ^{216}Ra, being higher in energy than both the 3^- and 5^- states, as a consequence of the high value of ε_p, the energy of the dipole bosons, probably associated with the lack of experimental data for the energy levels of this isotope. Phenomenologically, this can also be attributed to the near spherical shape of this nucleus, as it lies near a closed neutron shell ($N_{\text{shell}} = 126$, $N_{216} = 128$), and therefore the mechanism responsible of octupole vibrations mentioned in Ref. [39] might have a greater influence over this state. It is important to mention that we were not able to find studies in the radium isotopic chain that include this isotope on their calculations.

The nucleus ^{218}Ra shows perfect signs of a quadrupole vibrator, as their energy levels are all equidistant from each other. The same applies for the negative parity states, starting from the state 5^-. The same behavior can be seen in for ^{220}Ra, although in this isotope our calculated 2^+ states is slightly lower in energy than expected. It is also interesting to note the fact that the level 1^- is higher in energy than the 3^- state in the first nuclei, which is consistent with the recent experimental data in Ref. [39], in which, as stated previously for ^{216}Ra, the authors suggest that the origin of this behavior emerges from an octupole vibrational mechanism. From ^{220}Ra onwards, the first negative parity state correspond to the 1^- state, and the spacing between the states of the negative parity band appoximates qualitatively to an octupole rotor.

The spectra for ^{222,224,226}Ra is consistent with both a static quadrupole deformed shape, as the spacing between the positive parity states follows the rules for a rotor (equation (2.1.17)), and with a static octupole deformed shape, given the spacing between the negative parity states and the fact that from the state 5^- onwards, the positive and negative parity states alternate between both parities,

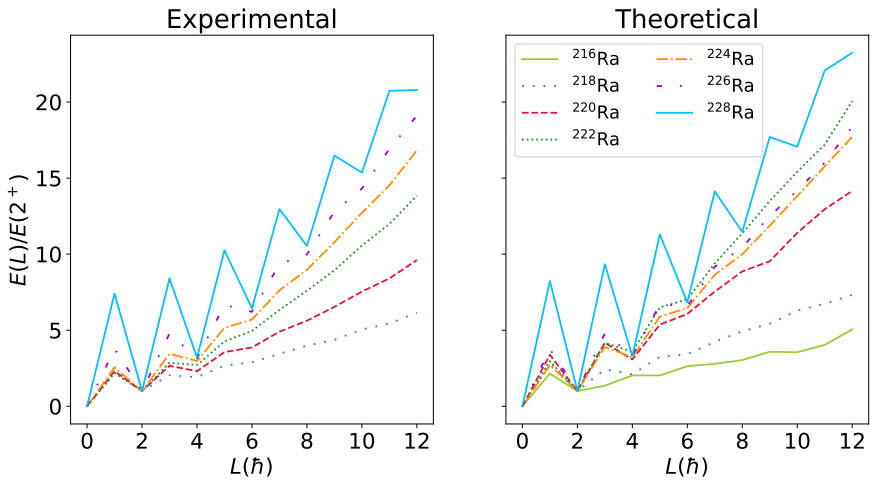

Figure 4.2.1: Experimental (left) and theoretical (right) energy ratios $E(L^\pi)/E(2^+)$ as function of the angular momentum L. The experimental staggering is not shown for ^{216}Ra given the lack of data available for its negative parity states.

becoming part of the same band.

Finally, we can observe that ^{228}Ra posseses a quadrupole deformed shape, although the negative parity band lies high in energy, appearing over the 6^+ state. This might be attributed to a vibrational mode, as the states do not form an alternating band and thus belong to different energy bands.

Following the analysis made in Ref. [7], we can observe the odd-even staggering present in each isotope in Fig. 4.2.1. A greater staggering is evidence of the positive and negative parity states belong to different bands, with the negative parity states forming their own rotational-like band, while a neglible staggering is evidence of a single band composed by states of different parity, or more specifically, two bands of different parity located close in energy. We can reproduce the experimentally observed staggering, which is clear in ^{228}Ra, while being less pronounced for ^{226}Ra.

Another phenomena that can be studied from the energy spectra is the emergence of octupole vibrational states, by calculating the energy displacement δE defined in Ref. [40] as

$$\delta E(L) = E(L^-) - \frac{E((L+1)^+) + E((L-1)^-)}{2}\,. \tag{4.2.1}$$

If the nucleus exhibits stable octupole deformation, δE would be near to zero, although this analysis does not inform us about the presence (or absence) of

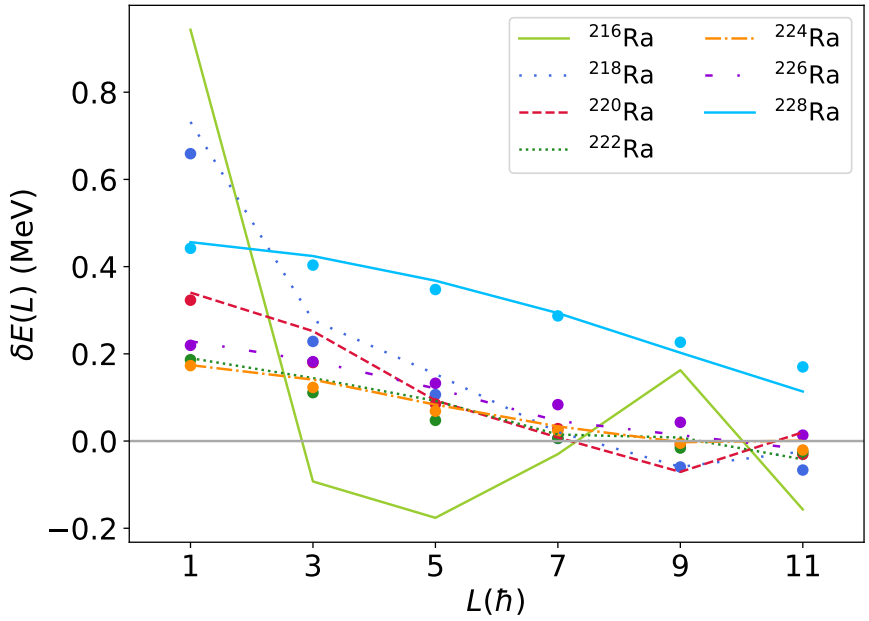

Figure 4.2.2: Evolution of the energy displacement in function of the angular momentum for the different isotopes of the chain. The experimental values are shown in markers, while the lines represent theoretical values. The gray horizontal line represents the limit for stable octupole deformation.

octupole vibrations. In figure 4.2.2 we plot the results.

It can be seen that our calculations reproduce quite well the experimental results, and it is clear that the results for $^{222-226}$Ra tend to a value of $\delta E \sim 0$ as the angular momentum increases. The results for ^{228}Ra are clear evidence of the absence of permanent octupole deformation in this nuclei, and the same can be said about the fluctuating behavior of ^{216}Ra.

One should note the special case of ^{218}Ra, in which the energy displacement rapidly decreases with the angular momentum, becoming negative for $L = 9$, with the experimental value continuing to decrease at $L = 11$, while our theoretical calculations show an increase at $L = 11$, with δE near zero, which would suggest that this nuclei would exhibit a static octupole shape. However, if one looks at the calculated energy levels, it is visible that our 12^+ state is lower in energy than the experimental value, which accounts to this behavior. Something similar can be said about ^{220}Ra, although its experimental value lies near zero, in a similar position to the one of ^{222,224}Ra, which suggests a static behavior as well.

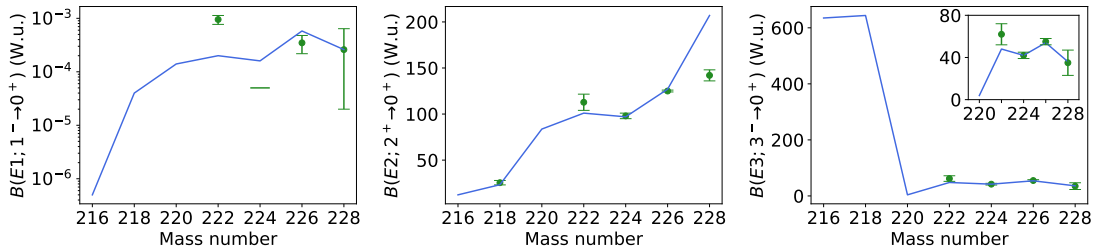

Figure 4.2.3: Electromagnetic transition rates $B(E\lambda; \lambda \rightarrow 0^+)$ for the isotopes of the chain. The results are provided in Weisskopf units. The horizontal line in ^{224}Ra represents a lower limit.

4.2.2 Electromagnetic Transitions

Regarding the electromagnetic transitions $B(E\lambda)$, we show the results for the transitions $B(E\lambda; \lambda \rightarrow 0)$ in figure 4.2.3. We make a zoom in the $B(E3; 3^- \rightarrow 0+)$ transitions to observe in more detail their behavior in the region of $^{220-228}$Ra, as the results for $^{216-218}$Ra are quite high in energy in comparison and thus difficult an adequate contrast with the experimental data. We can observe that the calculated $B(E2)$ and $B(E3)$ transitions are in great agreement with the experimental data and the expected trends, while the $B(E1)$ transitions are in adequate orders of magnitude, although not as accurate compared to the other transitions.

The experimental data for $B(E1)$ and $B(E3)$ transitions was retrieved from Ref. [5] for ^{224}Ra, from Ref. [16] for ^{226}Ra and from Ref. [6] and its supplementary material for ^{222,228}Ra. The experimental data for $B(E2)$ transitions was retrieved for the previously mentioned sources, as well from Ref. [34] for ^{216,218}Ra.

4.2.2.1 B(E1) transitions

For $B(E1)$ transition rates, we use the operator defined in equation (3.0.2) and an effective charge $e_1 = 0.0039$ [efm], constant for all nuclei in the chain. This value was chosen as the best fit that shows a better agreement with the order of magnitude of the available experimental data. The calculated transitions were from the type $L^{\pm} \rightarrow (L-1)^{\mp}$ based on the available experimental data. The results are presented in table 4.2.1 and compared in figure 4.2.4 for the isotopes with experimental results.

We can observe that there is a reasonable agreement between the experimental and theoretical results, specially for the $1^- \rightarrow 0^+$ transitions. The really low values

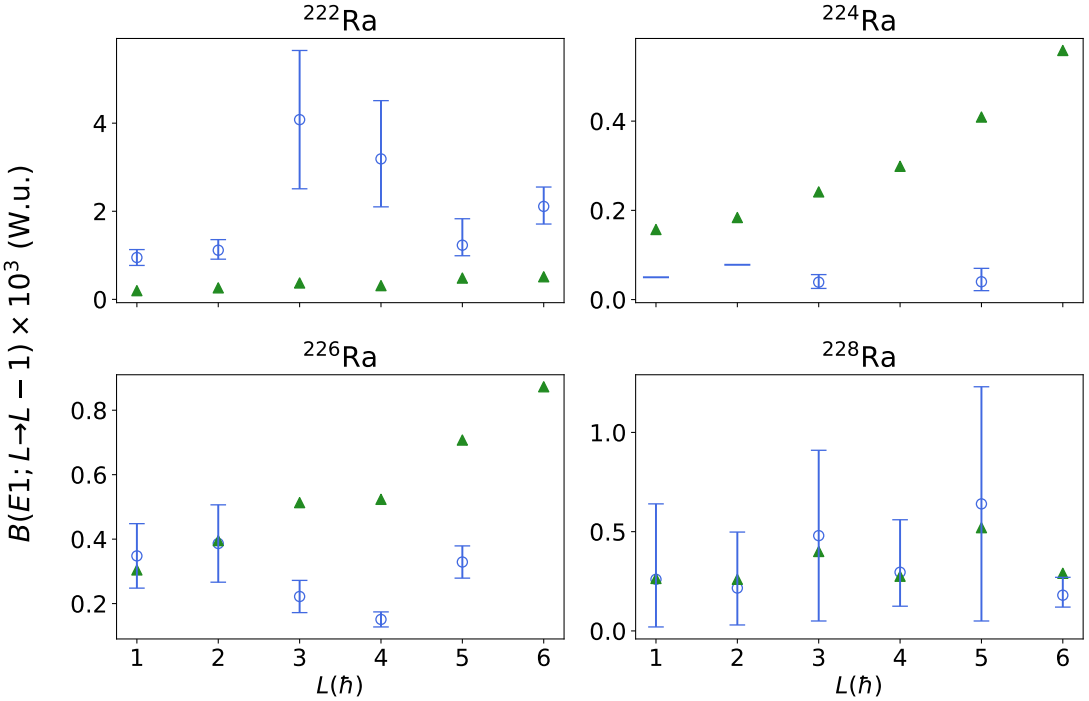

Figure 4.2.4: Comparison between the experimental (circle, in blue) and theoretical (triangle, in green) values for the $B(E1)$ transition rates, in Weisskopf Units. The horizontal blue lines represent upper experimental limits. The experimental values were taken from Refs. [4, 5, 16].

of $1^- \to 0^+$ transitions for ^{216}Ra might be attributed to the lack of experimental data available for this nucleus regarding this type of transitions, as well as a consequence of the small boson space available for our calculations, limiting an adequate description of the behavior in this nuclei.

The results for ^{218,220}Ra are in the expected orders of magnitude for dipole transitions, at least for the transitions at low levels. Our calculations for ^{222}Ra are an order of magnitude below the experimental results, which may be attributed to low collective effects in comparison with the next, heavier isotopes in the chain. This might be accounted for by using a different effective charge for this isotope, as it is made in Ref. [9], but we decided to use a constant charge along the whole chain.

We would like to point out the great accuracy observed for ^{228}Ra at all values of angular momentum, which may be a consequence of the above mentioned collective effects, and also a result of the fitting process priorizing these transitions, given that in comparison with the other isotopes studied, the dipole interactions

and their trends are in a better agreement with the experimental data than the quadrupole and octupole interactions.

4.2.2.2 B(E2) transitions

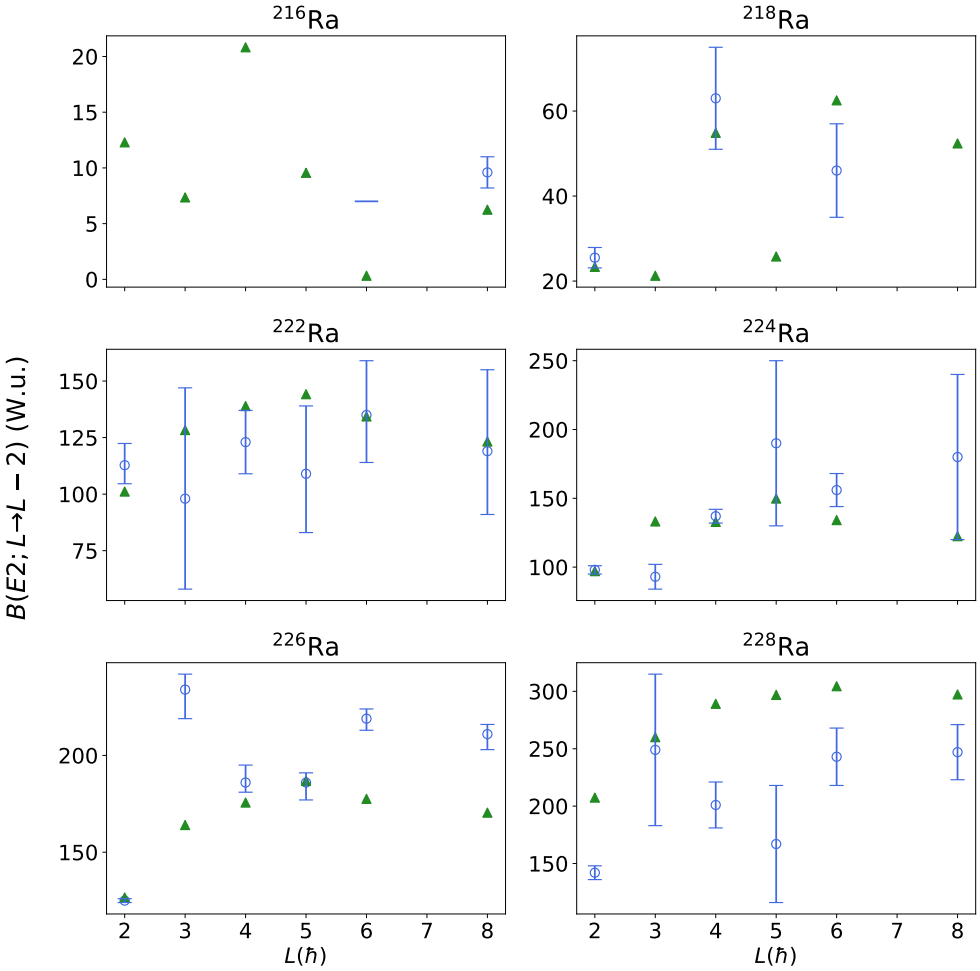

Figure 4.2.5: Comparison between the experimental (circle, in blue) and theoretical (triangle, in green) values for the $B(E2)$ transition rates, in Weisskopf Units. The horizontal blue lines represent lower experimental limits. The experimental values were taken from Refs. [4, 5, 16, 34].

With regards to the $B(E2)$ transition rates, we chose an effective charge $e_2 = 14.3$ [efm^2], in the same order of magitude than the common $e_2 = 18$ [efm^2] found in the literature, as well as the $\hat{Q}^{(2)}$ operator defined in equation (3.0.3). All the transitions calculated were of the type $L^{\pm} \rightarrow (L-2)^{\pm}$. The results are presented in table 4.2.2 and compared in figure 4.2.5 for the isotopes with experimental data available.

We can observe that the predictions of the $B(E2; 2^+ \rightarrow 0^+)$ states are in a reasonable agreement with the experimental data for all the nuclei except ^{228}Ra, which is highly overestimated. We observe that the value of these transitions get higher with the mass number, which is consistent with the higher collective effects observed in nuclei far from the closed neutron shell.

In the nuclei with more experimental data available, our results tend to maximize on the $5^- \rightarrow 3^-$ transition, after which they decrease in value for the next angular momenta. This was also observed in Ref. [41], where is proposed that this behavior might be related the nature of the model.

It is interesting to observe that our calculated transitions show a smoother behavior with the angular momentum in comparison with the experimental data, in the sense that the results do not fluctuate as much as the data does. This might be attributed to a limitation of the model, as it can be seen in Ref. [19] where the limiting cases of the dynamical symmetries in the *sd*-IBM-1, the $B(E2)$ transitions for the vibrational and rotational limits follow an inverted parabola as function to the angular momentum, respectively given by

$$B(E2; L+2 \rightarrow L)_{\text{vib}} \sim (L+2)(2N-L)\,, \tag{4.2.2}$$

$$B(E2; L+2 \rightarrow L)_{\text{rot}} \sim (2N-L)(2N+L+8)\,, \tag{4.2.3}$$

where N is the number of bosons present in the nucleus.

4.2.2.3 B(E3) transitions

In this case, we utilized an effective charge $e_3 = 300$ [efm^3] and the $\hat{Q}^{(3)}$ operator from equation (3.0.4). We calculated transitions of the type $L^- \rightarrow (L-3)^+$ and $L^{\pm} \rightarrow (L-1)^{\mp}$ given the available data. Our calculations are presented in table 4.2.3 and compared in figure 4.2.6 for the isotopes with experimental results.

We can see that the $B(E3; 3^- \rightarrow 0^+)$ transition rates are in great agreement with the experimental data for all nuclei in which it is available, and for the other $B(E3; L \rightarrow L-3)$ our results follow the trend of the experiments, except for ^{228}Ra.

We are not currently capable, however, of reproducing the expected behavior for ^{216,218}Ra, obtaining results that are higher than even the nuclei with permanent

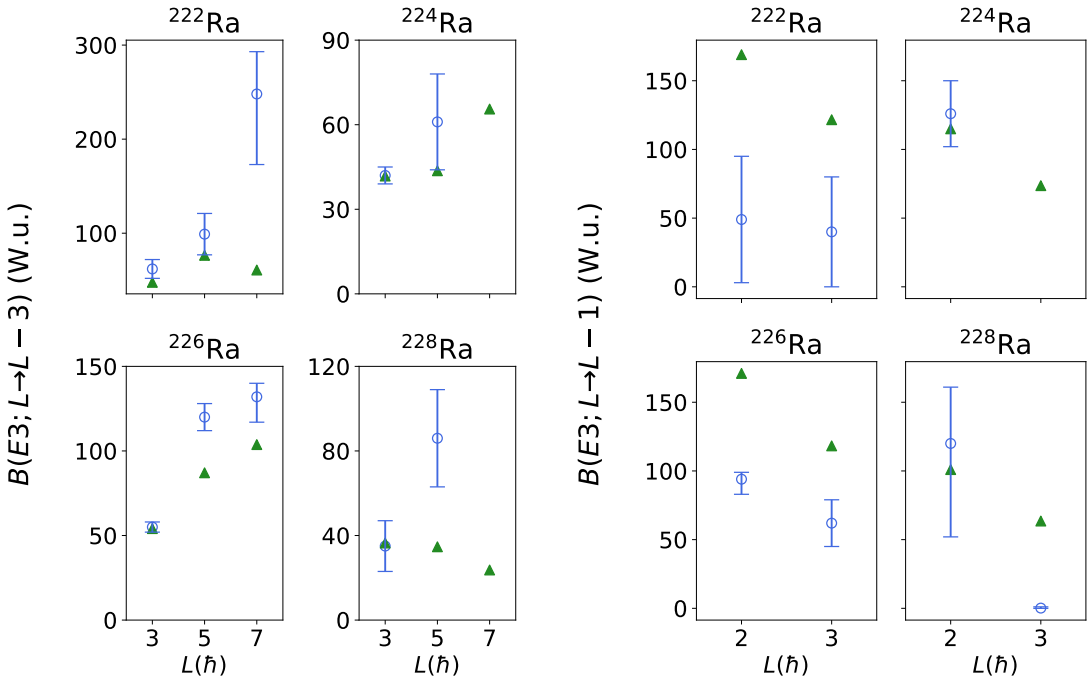

Figure 4.2.6: Comparison between the experimental (circle, in blue) and theoretical (triangle, in green) values for the $B(E3)$ transition rates, in Weisskopf Units. We present the values for the $B(E3; L \to L-3)$ transitions for $L = 3, 5, 7$ and the $B(E3; L \to L-1)$ for $L = 1, 3$. The experimental values were taken from Refs. [4, 5, 16].

octupole deformation. We attribute these values to a limitation of the hamiltonian used in this work, as we can observe a value for κ_1 in ^{216}Ra, a nuclei near the closed neutron shell, similar to that of ^{226}Ra, a nuclei far from the closed shell and expected to be octupole deformed. Therefore, we do not consider these calculations to be adequate predictions for those nuclei.

In the case of ^{220}Ra, our results consist on low values for the $L \to L-3$ transitions that suggest the absence of octupole deformation, which is in direct contrast with what was discussed in relation to the behavior of its energy displacement. However, in Ref. [6] is discussed that the observation of near-zero $B(E3)$ values for some but not all transitions, might be consistent with an octupole vibrational shape.

4.2.3 Intrinsic Octupole Moments

We present in figure 4.2.7 a plot for the calculated Q_3 intrinsic octupole moments for all the isotopes on the chain, calculated using equation (3.2.2). According

to Refs. [1, 2], the octupole vibrator limit occurs for values near the measured moment of ^{208}Pb, around 2100 [efm^3], which is represented bu the red dotted line.

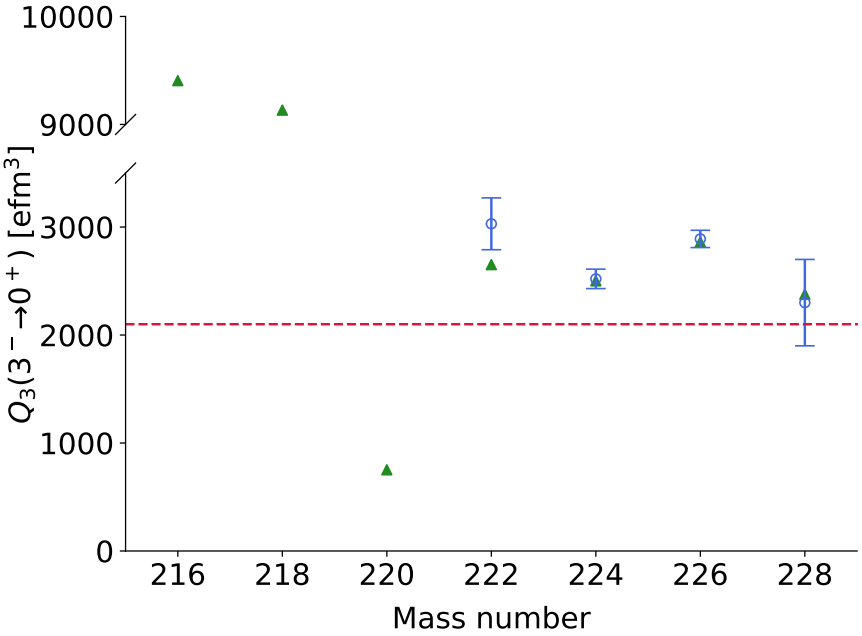

Figure 4.2.7: Intrinsic octupole moments Q_3 for the $3^- \rightarrow 0^+$ transition. The green triangles correspond to our theoretical calculations, while the blue circles correspond to experimental measures, reported in Ref. [6] for ^{222,228}Ra and in Ref. [5] for ^{224,226}Ra. The moments are in units of efm^3. The dotted red line corresponds to the limit of octupole vibration, deduced from the value of the octupole moment of ^{208}Pb, according to Refs. [1, 2].

The first remarkable feature that can be observed is the really high values of the moment for ^{216,218}Ra, as a consequence of the high $B(E3)$ values previously discussed. We must recall that we do not consider that these results should be taken as reliable, as we suppose that they are a consequence of an inadequate hamiltionian more than an accurate description of the phenomena occurring in these nuclei.

The low value of the moment for ^{220}Ra suggests that this nuclei should not exhibit octupole deformation, being better described as having a shape with really small octupole vibrations around a quadrupole deformed equilibrium shape, again consistent with the low value of the $B(E3)$ transition in single particle units.

For the nuclei with experimental data available, we can again observe that our calculations show great agreement with them. The results are consistent with the expected behavior of $^{222-226}$Ra, which according to the literature is a static octupole

shape. In the case of ^{228}Ra, it is believed to present octupole vibrations over a static quadrupole equilibrium shape, an idea reinforced by the error bars of the experimental measure, having the posibility of being closer to the vibrational limit. Given that our calculated moment is really close to the experimental measures, and in consistency with the energy spectrum of this nucleus, we conclude that our calculations also allow us to classify it as an octupole vibrator.

4.3 Influence of the multipole terms on the hamiltonian.

As can be seen in table 4.1.1, the κ_3 parameter is zero for all the isotopes in the chain, which implies that the octupole interaction is not relevant to the description of octupole phenomena when there already exists an interaction that mixes the parity of the different states, this being the dipole interaction. This is consistent with the behavior observed by Ref. [9], where their hamiltonian only includes dipole and quadrupole interactions.

For this discussion, we turn off the dipole interaction in ^{224}Ra by making $\kappa_1 = 0$, while keeping the other parameters constant. The comparison between the energy spectra is presented in figure 4.3.1, and the transition rates are presented in table 4.3.1.

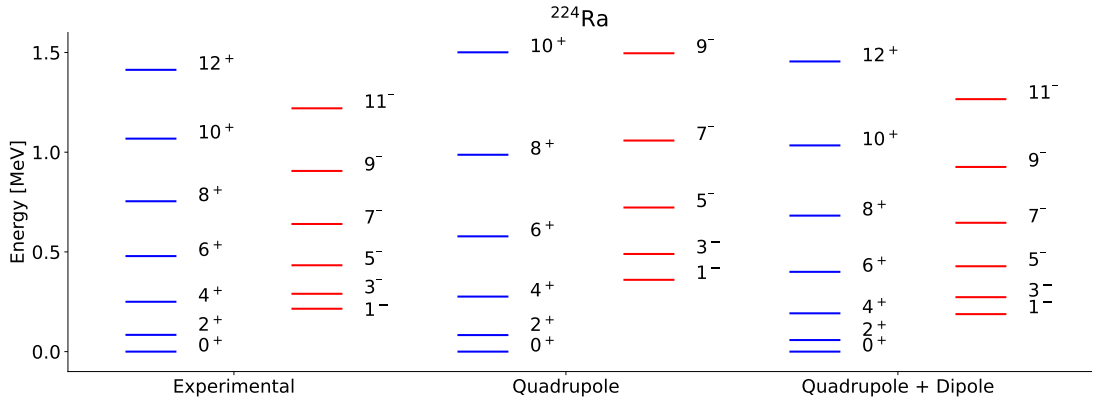

Figure 4.3.1: Comparison between the experimental and theoreticals energy levels of ^{224}Ra in the presence or absence of the dipole interaction. The experimental data is from Ref. [34].

It can be observed that in absence of the dipole interaction, the energy spectra of the positive parity states still corresponds to the one of a quadrupole deformed

shape, given the position of the 2^+ and 4^+ states, corresponding to a ratio $R_{4/2} \sim 3.3$. In fact, this quadrupole shape survives at higher spin, as the spacing between the higher levels of positive parity follows the $L(L+1)$ energy of a rotor, although with a lower moment of inertia than in the experimental results. This behavior implies that the dipole interaction increases the moment of inertia of the nucleus, according to equation (2.1.17). In regards to the negative parity states, these emerge at a higher energy, also showing a behavior similar to an octupole rotor given the space between them, and together with the positive parity states they do not follow the sequence $5^-, 6^+, 7^-, \ldots$, meaning that the states of different parity are not part of the same band.

Therefore, the inclusion of the dipole interaction seems to be responsible of the lowering of the energy of the negative parity states, as well as having an effect in the behavior of the high spin positive parity states, changing the shape of the nuclei at them, and allowing the alternation of the positive and negative parity states from 5^- onwards, so the states become part of the same band.

In the case of the transition rates, it is particularly interesting the behavior of the $B(E1)$ transitions, as the theoretical value in absence of the dipole interaction is more consistent with the experimental data than the case without it. This might be evidence of the need for the inclusion of a new term in the hamiltonian, different from the octupole interaction, which may be needed for a better description of the $B(E1)$ transition rates which, as discussed in Ref. [1], are more sensible to microscopic considerations.

The $B(E2)$ transitions seem to not be affected by the introduction of the dipole interaction, keeping the results in the same order of magnitude of those including the interaction. This behavior is expected, as the quadrupole transitions should not be greatly affected by the introduction of an interaction of different multipole, less if this interaction represents a transition with different parity.

Finally, we observe that the $B(E3)$ transitions are greatly diminished without the dipole interaction. This is probably attributed to the difficulty of describing phenomena asociated with odd multipoles without an interaction of that kind.

For the sake of comparison, we also made calculations including an octupole interaction ($\kappa_3 \neq 0$) while fixing the dipole interaction to zero. For this, we used the parameters presented in table 4.1.1 for ^{224}Ra as a seed except for κ_1 which,

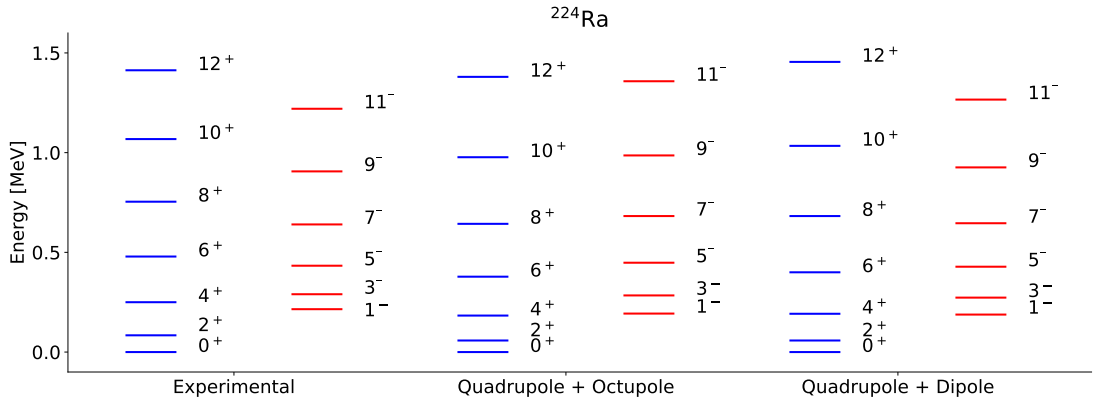

Figure 4.3.2: Comparison between the experimental and theoretical energy levels of ^{224}Ra in the presence of quadrupole and dipole interactions, and quadrupole and octupole interactions. The experimental data is from Ref. [34].

as said above, was fixed to zero. This resulted in the parameters shown in table 4.3.2. The energy spectra and electromagnetic transitions are presented in figure 4.3.2 and in table 4.3.3, respectively.

We can observe a lowering in the energy of both the positive and negative parity states. This is specially visible for the positive parity states, that although they conserve the behavior of a quadrupole rotor, it seems that the moment of inertia of the nuclear shape has been increased given the distance between different states. On the negative parity band, on the other hand, the behavior is similar than the discussed when only considering the quadrupole interaction, so the negative parity states do not become part of a single band of alternating parity with the positive parity states.

Regarding the electromagnetic transition rates, we again observe a similar behavior for the $B(E1)$ transition rates, being more consistent with the same order of magnitude than the experimental data in comparison with the case of quadrupole and dipole interaction. However, the calculations for the $B(E2)$ transitions are greatly enhanced, being most of them in the order of 200 Weisskopf units, far off the experimental results. The $B(E3)$ transitions have a similar behavior for the $L \to (L-3)$ transitions, presenting results on the order of 100 single particle units, while being lower than the calculations with the quadrupole and dipole interactions in the transitions of the type $L \to (L-1)$.

Given the discussion about the effects of the octupole interaction, specially over the transition rates, it suggests that this interaction does not describe the octupole

degrees of freedom as well as the dipole interaction used in this work.

$B(E1)$ Transition	^{216}Ra		^{218}Ra		^{220}Ra	
($\times 10^{-3}$)	Exp	Theo	Exp	Theo	Exp	Theo
$1^- \to 0^+$	-	0.0005	-	0.04	-	0.14
$2^+ \to 1^-$	-	0.0001	-	0.006	-	0.096
$3^- \to 2^+$	-	0.19	-	0.13	-	0.23
$4^+ \to 3^-$	-	0.004	-	0.0001	-	0.14
$5^- \to 4^+$	-	0.034	-	0.26	-	0.42
$6^+ \to 5^-$	-	0.319	5.7 ± 1.7	0.0013	-	0.23

$B(E1)$ Transition	^{222}Ra		^{224}Ra		^{226}Ra	
($\times 10^{-3}$)	Exp	Theo	Exp	Theo	Exp	Theo
$1^- \to 0^+$	0.95 ± 0.18	0.20	< 0.05	0.158	0.35 ± 0.13	0.58
$2^+ \to 1^-$	$1.12^{+0.24}_{-0.20}$	0.26	< 0.078	0.185	0.38 ± 0.11	0.76
$3^- \to 2^+$	4.08 ± 1.57	0.37	$0.039^{+0.017}_{-0.014}$	0.243	0.22 ± 0.05	0.98
$4^+ \to 3^-$	$3.19^{+1.3}_{-1.1}$	0.31	-	0.303	0.15 ± 0.02	1.00
$5^- \to 4^+$	$1.23^{+0.60}_{-0.24}$	0.48	$0.04^{+0.03}_{-0.02}$	0.413	0.33 ± 0.05	1.36
$6^+ \to 5^-$	$2.11^{+0.44}_{-0.40}$	0.51	-	0.566	-	1.67

$B(E1)$ Transition	^{228}Ra	
($\times 10^{-3}$)	Exp	Theo
$1^- \to 0^+$	$0.26^{+0.38}_{-0.24}$	0.26
$2^+ \to 1^-$	$0.32^{+0.28}_{-0.19}$	0.26
$3^- \to 2^+$	0.048 ± 0.43	0.40
$4^+ \to 3^-$	$0.30^{+0.26}_{-0.17}$	0.27
$5^- \to 4^+$	0.64 ± 0.59	0.52
$6^+ \to 5^-$	$0.018^{+0.09}_{-0.06}$	0.29

Table 4.2.1: Transition rates for the electric dipole transitions $B(E1)$. The results are presented in Weisskopf units. A dash represent the fact that no experimental data was available for that transition.

$B(E2)$ Transition	^{216}Ra		^{218}Ra		^{220}Ra	
	Exp	Theo	Exp	Theo	Exp	Theo
$2^+ \to 0^+$	-	12.3	25.5 ± 2.4	23.3	-	83.7
$4^+ \to 2^+$	-	20.8	63 ± 12	54.9	-	110.4
$6^+ \to 4^+$	> 7.0	0.3	46 ± 11	62.5	-	105.5
$8^+ \to 6^+$	9.6 ± 1.4	6.3	-	52.4	-	78.1
$3^- \to 1^-$	-	7.4	-	21.3	-	104.2
$5^- \to 3^-$	-	9.6	-	25.8	-	110.8

$B(E2)$ Transition	^{222}Ra		^{224}Ra		^{226}Ra	
	Exp	Theo	Exp	Theo	Exp	Theo
$2^+ \to 0^+$	$112.8^{+9.6}_{-8.2}$	101	98 ± 3	97	125 ± 1	127
$4^+ \to 2^+$	123 ± 14	139	137 ± 5	133	186^{+9}_{-5}	176
$6^+ \to 4^+$	135^{+24}_{-21}	134	156 ± 12	134	219^{+5}_{-6}	178
$8^+ \to 6^+$	119^{+36}_{-28}	123	180 ± 60	122	211^{+5}_{-8}	170
$3^- \to 1^-$	98^{+49}_{-40}	128	93 ± 9	133	234^{+8}_{-15}	164
$5^- \to 3^-$	109^{+30}_{-26}	144	180 ± 60	150	186^{+5}_{-9}	187

$B(E2)$ Transition	^{228}Ra	
	Exp	Theo
$2^+ \to 0^+$	142 ± 6	207
$4^+ \to 2^+$	201 ± 20	289
$6^+ \to 4^+$	243 ± 25	305
$8^+ \to 6^+$	247 ± 24	297
$3^- \to 1^-$	249 ± 66	260
$5^- \to 3^-$	167^{+34}_{-69}	297

Table 4.2.2: Transition rates for the electric quadrupole transitions $B(E2)$. The results are presented in Weisskopf units. A dash represent the fact that no experimental data was available for that transition.

$B(E3)$ Transition	^{216}Ra		^{218}Ra		^{220}Ra	
	Exp	Theo	Exp	Theo	Exp	Theo
$3^- \to 0^+$	-	635	-	644	-	3.9
$5^- \to 2^+$	-	443	-	358	-	1.0
$7^- \to 4^+$	-	285	-	236	-	1.5
$2^+ \to 1^-$	-	108	-	0.63	-	39.3
$3^- \to 2^+$	-	69.6	-	24.9	-	17.3

$B(E3)$ Transition	^{222}Ra		^{224}Ra		^{226}Ra	
	Exp	Theo	Exp	Theo	Exp	Theo
$3^- \to 0^+$	62 ± 10	48	42 ± 3	42	55 ± 3	54
$5^- \to 2^+$	99 ± 22	77	61 ± 17	44	120 ± 8	87
$7^- \to 4^+$	248^{+45}_{-75}	61	-	67	132^{+8}_{-15}	104
$2^+ \to 1^-$	49 ± 28	169	126 ± 24	115	94^{+5}_{-11}	171
$3^- \to 2^+$	40^{+44}_{-40}	122	< 600	74	62 ± 17	118

$B(E3)$ Transition	^{228}Ra	
	Exp	Theo
$3^- \to 0^+$	35 ± 12	36
$5^- \to 2^+$	86 ± 23	35
$7^- \to 4^+$	-	24
$2^+ \to 1^-$	120 ± 41	101
$3^- \to 2^+$	$0.17^{+0.9}_{-0.17}$	64

Table 4.2.3: Transition rates for the electric octupole transitions $B(E3)$. The results are presented in Weisskopf units. A dash represent the fact that no experimental data was available for that transition.

	^{216}Ra	^{218}Ra	^{220}Ra	^{222}Ra	^{224}Ra	^{226}Ra	^{228}Ra
Q_3 [efm^3]	9406	9133	752	2652	2502	2862	2378

Table 4.2.4: Calculated intrinsic Q_3 moments, in units of [efm^3].

Transition		Exp	$Q^{(2)}$	$Q^{(2)}+Q^{(1)}$
$B(E1)\times10^{-3}$ (W.u.)	$1^-\to0^+$	<0.050	0.033	0.158
	$2^+\to1^-$	<0.078	0.021	0.185
	$3^-\to2^+$	$0.039^{+0.017}_{-0.014}$	0.054	0.243
	$4^+\to3^-$	-	0.031	0.303
	$5^-\to4^+$	$0.04^{+0.03}_{-0.02}$	0.079	0.413
	$6^+\to5^-$	-	0.048	0.566
$B(E2)$ (W.u.)	$2^+\to0^+$	98 ± 3	101	97
	$4^+\to2^+$	137 ± 5	140	133
	$6^+\to4^+$	156 ± 12	144	134
	$8^+\to6^+$	180 ± 60	137	122
	$3^-\to1^-$	93 ± 9	137	133
	$5^-\to3^-$	190 ± 60	155	150
$B(E3)$ (W.u.)	$3^-\to0^+$	42 ± 3	21	42
	$5^-\to2^+$	61 ± 17	15	44
	$7^-\to4^+$	-	4	67
	$1^-\to2^+$	126 ± 24	70	115
	$3^-\to2^+$	<600	41	74

Table 4.3.1: Comparison for the electric transition rates of ^{224}Ra in the presence of only quadrupole interaction ($Q^{(2)}$) or a combination of the quadrupole and the dipole interactions ($Q^{(2)}+Q^{(1)}$). The experimental data is from Ref. [5].

	ε_d	ε_p	ε_f	κ_2	κ_1	κ_3	χ_d
^{224}Ra	0.263	0.800	0.459	0.030	0.0000	0.0068	-1.232

Table 4.3.2: Results obtained for ^{224}Ra considering quadrupole and octupole interactions.

Transition		Exp	$Q^{(2)}+Q^{(3)}$	$Q^{(2)}+Q^{(1)}$
$B(E1)\times 10^{-3}$ (W.u.)	$1^-\to 0^+$	< 0.050	0.043	0.158
	$2^+\to 1^-$	< 0.078	0.094	0.185
	$3^-\to 2^+$	$0.039^{+0.017}_{-0.014}$	0.089	0.243
	$4^+\to 3^-$	-	0.107	0.303
	$5^-\to 4^+$	$0.04^{+0.03}_{-0.02}$	0.088	0.413
	$6^+\to 5^-$	-	0.116	0.566
$B(E2)$ (W.u.)	$2^+\to 0^+$	98 ± 3	98	97
	$4^+\to 2^+$	137 ± 5	218	133
	$6^+\to 4^+$	156 ± 12	234	134
	$8^+\to 6^+$	180 ± 60	235	122
	$3^-\to 1^-$	93 ± 9	182	133
	$5^-\to 3^-$	190 ± 60	210	150
$B(E3)$ (W.u.)	$3^-\to 0^+$	42 ± 3	24	42
	$5^-\to 2^+$	61 ± 17	94	44
	$7^-\to 4^+$	-	112	67
	$2^+\to 1^-$	126 ± 24	77	115
	$3^-\to 2^+$	< 600	67	74

Table 4.3.3: Comparison for the electric transition rates of ^{224}Ra in the presence of quadrupole and dipole interactions ($Q^{(2)}+Q^{(1)}$), and the quadrupole and octupole interactions ($Q^{(2)}+Q^{(3)}$). The experimental data is from Ref. [5].

Chapter 5

Final Remarks

In this work we have obtained theoretical results for the spectroscopic properties of the $^{216-228}$Ra isotopic chain that are consistent with the experimental data currently available, in particular the energy spectra and the $B(E2)$ and $B(E3)$ transition rates. From the last ones via the derivation of intrinsic octupole moments Q_3 we can deduce the presence of static octupole deformation in $^{222-226}$Ra, and of vibrational deformation in ^{228}Ra.

The results presented for ^{220}Ra are consistent with the behavior reported in the literature for the electromagnetic transitions in this region of the nuclear chart, and thus we present them as predictions, suggesting an octupole vibrational shape for this isotope.

The results obtained for the isotopes ^{216,218}Ra are not consistent with the expected behavior deduced from the theory, as these nuclei are near a closed neutron shell and thus should not exhibit signs of octupole deformation, in contrast with the Q_3 moments of around 9000 [efm^3] obtained by our calculations. This suggests that the hamiltonian that we used during this work might be adequate for the description of deformed nuclei, but not for the description of lighter nuclei, as we were not capable of finding a set of parameters in these nuclei that give a reasonable description of their electromagnetic transitions, possibly associated with the lack of experimental data available for them.

Regarding the $B(E1)$ values calculated, improvements may be achieved with the use of an effective charge that evolves along the isotopic chain, or by including a new interaction in our hamiltonian instead of the octupole interaction, given that

this term does not contribute to the calculated results. However, these calculations are still of a reasonable accuracy overall, considering that the dipole transitions are more dependent on the inner structure of each nucleus. This new interaction might also help to improve the results for the $B(E3)$ transitions in ^{216,218}Ra to something more in line with the expected behavior in the mass region.

We remark the fact that these calculations were made with a simple choice for the hamiltonian and only seven (six) free parameter, where one of them seems to not be relevant in the description of the octupole degrees of freedom. This success takes us to propose that the minimization routine and the hamiltonian applied for the radium chain in the context of the model might be applied to other chains within the actinide region, like thorium, where there is also more experimental data available.

As further work we would like to study the boson content of each state, which may give us a better explanation for the behavior of some of the transitions, and also study possible interactions that may account for the previously discussed new interaction. Another viable posibility is to change the definition of our $\hat{Q}^{(2)}$ operator to be more similar to the one discussed in Ref. [21] including an α parameter, the relative weight between the sd and pf parts of this operator shown in equation (2.2.17), as a free parameter in our hamiltonian.

References

[1] P. A. Butler, "Octupole collectivity in nuclei", Journal of Physics G: Nuclear and Particle Physics **43**, 073002 (2016).

[2] P. A. Butler, "Pear-shaped atomic nuclei", Proceedings of the Royal Society A: Mathematical, Physical and Engineering Sciences **476**, 20200202 (2020).

[3] K. Nomura, "Signatures of octupole shape phase transitions in radioactive nuclei", Journal of Physics: Conference Series **1643**, 012152 (2020).

[4] P. A. Butler, L. P. Gaffney, P. Spagnoletti, et al., "The observation of vibrating pear-shapes in radon nuclei", Nature Communications **10**, 2473 (2019).

[5] L. P. Gaffney, P. A. Butler, M. Scheck, et al., "Studies of pear-shaped nuclei using accelerated radioactive beams", Nature **497**, 199–204 (2013).

[6] P. A. Butler, L. P. Gaffney, P. Spagnoletti, et al., "Evolution of Octupole Deformation in Radium Nuclei from Coulomb Excitation of Radioactive Ra 222 and Ra 228 Beams", Physical Review Letters **124**, 042503 (2020).

[7] K. Nomura, D. Vretenar, T. Nikšić, et al., "Microscopic description of octupole shape-phase transitions in light actinide and rare-earth nuclei", Physical Review C **89**, 024312 (2014).

[8] O. Vallejos and J. Barea, "Octupole and quadrupole modes in radon isotopes using the proton-neutron interacting boson model", Physical Review C **104**, 014308 (2021).

[9] N. V. Zamfir and D. Kusnezov, "Octupole correlations in the transitional actinides and the spdf interacting boson model", Physical Review C **63**, 054306 (2001).

[10] S. M. Wong, "Nuclear collective motion", in *Introductory nuclear physics* (John Wiley & Sons, Ltd, 1998) Chap. 6, pp. 205–234.

[11] W. Greiner and J. A. Maruhn, "Collective models", in *Nuclear models: with 39 worked examples and problems* (Springer, Berlin Heidelberg, 1996).

[12] P. A. Butler and W. Nazarewicz, "Intrinsic reflection asymmetry in atomic nuclei", Reviews of Modern Physics **68**, 349–421 (1996).

[13] A. Bohr and B. R. Mottelson, *Nuclear structure*, Vol. 2 (World Scientific Publishing Company, Jan. 1998).

[14] K. S. Krane and D. Halliday, "Nuclear models", in *Introductory nuclear physics* (Wiley, New York, 1987).

[15] A. Obertelli and H. Sagawa, "Deformation and rotation", in *Modern nuclear physics: from fundamentals to frontiers* (Springer Singapore, Singapore, 2021), pp. 461–533.
[16] H. Wollersheim, H. Emling, H. Grein, et al., "Coulomb excitation of ^{226}Ra", Nuclear Physics A **556**, 261–280 (1993).
[17] F. Iachello, ed., *Interacting Bosons in Nuclear Physics* (Springer US, Boston, MA, 1979).
[18] F. Iachello and A. Arima, "Part I: The interacting boson model-1. Operators", in *The interacting boson model*, Cambridge monographs on mathematical physics (Cambridge University Press, Cambridge; New York, 1987).
[19] F. Iachello and A. Arima, "Part I: The interacting boson model-1. Algebras", in *The interacting boson model*, Cambridge monographs on mathematical physics (Cambridge University Press, Cambridge; New York, 1987).
[20] O. Scholten, F. Iachello, and A. Arima, "Interacting boson model of collective nuclear states III. the transition from SU(5) to SU(3)", Annals of Physics **115**, 325–366 (1978).
[21] C. Alonso, J. Arias, A. Frank, et al., "Description of octupole-deformed nuclei within the interacting boson and interacting boson-fermion models", Nuclear Physics A **586**, 100–124 (1995).
[22] F. Iachello and A. Arima, "Boson symmetries in vibrational nuclei", Physics Letters B **53**, 309–312 (1974).
[23] A. Arima and F. Iachello, "Interacting boson model of collective states I. The vibrational limit", Annals of Physics **99**, 253–317 (1976).
[24] A. Arima and F. Iachello, "Interacting boson model of collective nuclear states II. The rotational limit", Annals of Physics **111**, 201–238 (1978).
[25] F. Iachello and A. Arima, "The interacting boson models-G, -F, -CM", in *The interacting boson model*, Cambridge monographs on mathematical physics (Cambridge University Press, Cambridge; New York, 1987).
[26] S. G. Rohozinski, "The oscillator basis for octupole collective motion in nuclei", Journal of Physics G: Nuclear Physics **4**, 1075–1099 (1978).
[27] K. Nomura, D. Vretenar, T. Nikšić, et al., "Microscopic description of octupole shape-phase transitions in light actinide and rare-earth nuclei", Physical Review C **89**, 024312 (2014).
[28] K. Nomura, R. Rodríguez-Guzmán, Y. M. Humadi, et al., "Octupole correlations in light actinides from the interacting boson model based on the Gogny energy density functional", Physical Review C **102**, 064326 (2020).
[29] J. Engel and F. Iachello, "Interacting boson model of collective octupole states", Nuclear Physics A **472**, 61–84 (1987).
[30] T. Otsuka and M. Sugita, "Unified description of quadrupole-octupole collective states in nuclei", Physics Letters B **209**, 140–144 (1988).
[31] D. Kusnezov, "The $U(16)$ algebraic lattice", Journal of Physics A: Mathematical and General **22**, 4271–4280 (1989).
[32] D. Kusnezov, "The $U(16)$ algebraic lattice. II. Analytic construction", Journal of Physics A: Mathematical and General **23**, 5673–5694 (1990).

[33] S. Kuyucak and M. Honma, "Mean field study of the quadrupole-octupole degree of freedom in the spdf boson model", Physical Review C **65**, 064323 (2002).
[34] International Atomic Energy Agency, *Livechart - Table of Nuclides - nuclear structure and decay data*, Retrieved September 9th, 2023.
[35] S. Heinze, *Computer program ARBMODEL*, Unpublished, 2008.
[36] H. Dembinski and P. O. et al., "Scikit-hep/iminuit", 10.5281/zenodo.3949207 (2020).
[37] F. James and M. Roos, "Minuit - a system for function minimization and analysis of the parameter errors and correlations", Computer Physics Communications **10**, 343–367 (1975).
[38] P. A. Contreras-Corral, *Sparse-IBM-Calc*, version 1.0, Mar. 2024.
[39] E. Parr, J. F. Smith, P. T. Greenlees, et al., "Identification of the $J^\pi = 1^-$ state in ^{218}ra populated via α decay of ^{222}th", Physical Review C **94**, 014307 (2016).
[40] W. Nazarewicz and P. Olanders, "Rotational consequences of stable octupole deformation in nuclei", Nuclear Physics A **441**, 420–444 (1985).
[41] O. Vallejos, "Estudio sistemático de la cadena de isótopos 214-224Rn en el marco de trabajo del IBM2", Master Thesis (Universidad de Concepción, Concepción, Chile, Nov. 2020).
[42] J. J. Sakurai and J. Napolitano, "Theory of angular momentum", in *Modern quantum mechanics*, 2nd ed (Addison-Wesley, Boston, 2011).
[43] A. De Shalit and I. Talmi, "Vector adition coefficients", in *Nuclear shell theory*, Vol. 14, Pure and Applied Physics: A Series of Monographs and Textbooks (Academic Press, New York; London, 1963).

Appendix A

Mathematical Elements

A.1 Spherical Tensors

The spherical tensors are elements that transform under rotations as a wavefunction with good angular momentum [11]. A (irreducible) spherical tensor with k units of angular momentum, $T^{(k)}$, possesses $2k+1$ components $T^{(k)}_q$, where $q = -k, \ldots, k$. Under a rotation $\mathscr{R}$ it transforms according to the following expression

$$T'^{(k)}_q = \sum_{q'=-k}^{k} T^{(k)}_{q'} \mathscr{D}^{(k)}_{q',q}(\mathscr{R}) \,, \tag{A.1.1}$$

where the $\mathscr{D}(\mathscr{R})$ matrices are the $(2j+1)$-dimensional irreducible representations of the rotation operator $\mathscr{R}(\theta)$ [42], and their matrix elements $\mathscr{D}^{(j)}_{m',m}(\mathscr{D})$, sometimes called Wigner functions, satisfy

$$\mathscr{D}^{(j)}_{m',m}(\mathscr{R}) = \langle jm'|\mathscr{R}(\theta)|jm\rangle \ . \tag{A.1.2}$$

These tensors allow the definition of the tensor products used in the IBM, for which we shall use the notation of De Shalit and Talmi, this is,

$$T^{(k)}_\kappa = \left[T^{(k_1)} \times T^{(k_2)}\right]^{(k)}_\kappa = \sum_{\kappa_1,\kappa_2} (k_1\kappa_1 k_2\kappa_2|k\kappa) T^{(k_1)}_{\kappa_1} T^{(k_2)}_{\kappa_2} \,, \tag{A.1.3}$$

where $(k_1\kappa_1 k_2\kappa_2|k\kappa)$ corresponds to a Clebsch-Gordan coefficient. The special

case in which $k = 0 = \kappa$ corresponds to the scalar (or dot) product, defined as

$$\left(U^{(k)} \cdot V^{(k)}\right) = (-1)^k \sqrt{2k+1}\left[U^{(k)} \times V^{(k)}\right]_0^{(0)} . \tag{A.1.4}$$

A.2 The Wigner-Eckart Theorem

The Wigner-Eckart theorem establishes that the matrix elements of spherical tensor operators satisfy

$$\langle \alpha L M | T_q^{(k)} | \beta L' M' \rangle = (-1)^{L-M} \begin{pmatrix} L & k & L' \\ -M & q & M' \end{pmatrix} \langle \alpha L || T^{(k)} || \beta L' \rangle , \tag{A.2.1}$$

where we use the definition of De Shalit and Talmi used in Ref. [25]. Here, α and β are quantum numbers that may be needed to fully define each state, L, L' are the angular momentum quantum number, M, M' are the projection of the angular momentum on the z axis, $\langle \alpha L || T^{(k)} || \beta L' \rangle$ correspond to a reduced matrix element, and the 2×3 array corresponds to a $3j-$Wigner symbol, which is defined as [43]

$$\begin{pmatrix} L & k & L' \\ -M & q & M' \end{pmatrix} = \frac{(-1)^{L-k-M'}}{\sqrt{2L'+1}} (L(-M)kq|L'(-M')) , \tag{A.2.2}$$

where the $(L(-M)kq|L'(-M'))$ is a Clebsch-Gordan coefficient.

The significance of this theorem, according to the discussion in Ref. [42] , comes from the two factors that compose it. The first factor, the $3j-$Wigner symbol, is related to the Clebsch-Gordan coefficients, so it depends only on the orientation of the system and not on the nature of the tensor operator. The second factor, the reduced matrix element, depends on the dynamics of the system $(\alpha, \beta, L, L', k)$, and has no dependence on the M, M' projections of the angular momenta on the z axis nor on the q component of the tensor (the geometry of the system). Therefore, to evaluate the matrix element it is necessary to know about the dynamics of the system and only one of the geometric quantum numbers, as the other can be obtained by the Clebsch-Gordan coefficients.